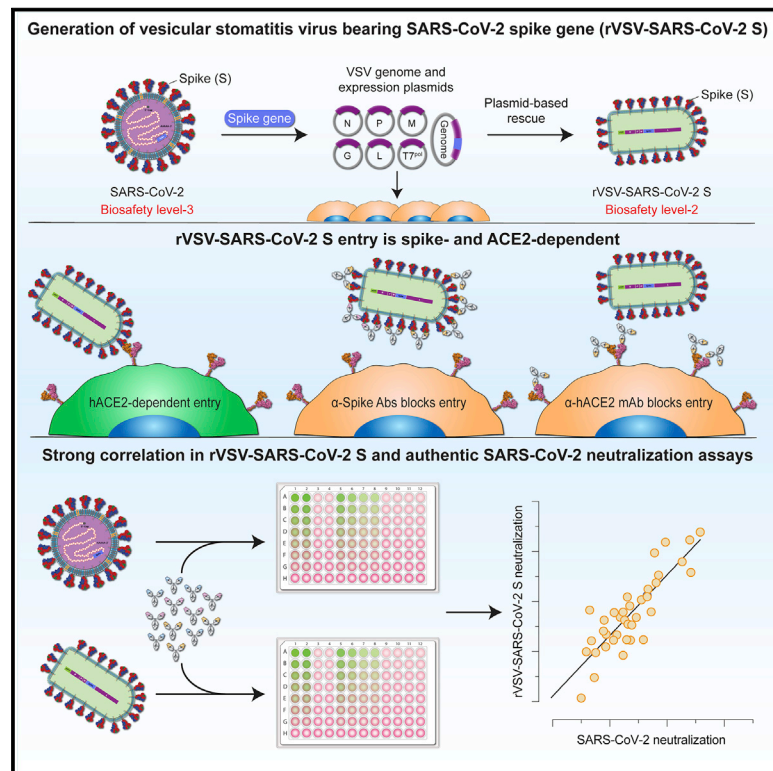# Cell Host & Microbe

A Replication-Competent Vesicular Stomatitis Virus for Studies of SARS-CoV-2 Spike-Mediated Cell Entry and Its Inhibition

Graphical Abstract

Authors

M. Eugenia Dieterle,
Denise Haslwanter,
Robert H. Bortz III, ...,
Andrew S. Herbert, Kartik Chandran,
Rohit K. Jangra

Correspondence

andrew.s.herbert4.ctr@mail.mil (A.S.H.),
kartik.chandran@einsteinmed.org (K.C.),
rohit.jangra@einsteinmed.org (R.K.J.)

In Brief

Surrogate systems are needed to evaluate COVID-19 vaccines and therapeutics rapidly and at scale. Dieterle & Haslwanter et al. describe a highly infectious recombinant vesicular stomatitis virus encoding the SARS-CoV-2 spike protein that is suitable for screening and mechanistic studies of small molecule inhibitors, recombinant biologics, and convalescent plasma.

Highlights

- Highly infectious recombinant VSV expressing SARS-CoV-2 spike (S) was generated

- rVSV-SARS-CoV-2 S resembles SARS-CoV-2 in entry and inhibitor or antibody sensitivity

- rVSV-SARS-CoV-2 S affords rapid screens and forward-genetic analyses of antivirals

CellPress

Resource

A Replication-Competent Vesicular Stomatitis Virus for Studies of SARS-CoV-2 Spike-Mediated Cell Entry and Its Inhibition

M. Eugenia Dieterle,[1,8] Denise Haslwanter,[1,8] Robert H. Bortz III,[1] Ariel S. Wirchnianski,[1,2] Gorka Lasso,[1] Olivia Vergnolle,[2] Shawn A. Abbasi,[3] J. Maximilian Fels,[1] Ethan Laudermilch,[1] Catalina Florez,[1,4] Amanda Mengotto,[5] Duncan Kimmel,[5] Ryan J. Malonis,[2] George Georgiev,[2] Jose Quiroz,[5] Jason Barnhill,[4] Liise-anne Pirofski,[1,5] Johanna P. Daily,[1,5] John M. Dye,[3] Jonathan R. Lai,[2] Andrew S. Herbert,[3,6,*] Kartik Chandran,[1,7,*] and Rohit K. Jangra[1,*]

[1]Department of Microbiology and Immunology, Albert Einstein College of Medicine, Bronx, NY 10461, USA
[2]Department of Biochemistry, Albert Einstein College of Medicine, Bronx, NY 10461, USA
[3]U.S. Army Medical Research Institute of Infectious Diseases, Frederick, MD 21702, USA
[4]Department of Chemistry and Life Science, United States Military Academy at West Point, West Point, NY 10996, USA
[5]Division of Infectious Diseases, Department of Medicine, Albert Einstein College of Medicine and Montefiore Medical Center, Bronx, NY 10461, USA
[6]The Geneva Foundation, 917 Pacific Avenue, Tacoma, WA 98402, USA
[7]Lead Contact
[8]These authors contributed equally
*Correspondence: andrew.s.herbert4.ctr@mail.mil (A.S.H.), kartik.chandran@einsteinmed.org (K.C.), rohit.jangra@einsteinmed.org (R.K.J.)
https://doi.org/10.1016/j.chom.2020.06.020

SUMMARY

There is an urgent need for vaccines and therapeutics to prevent and treat COVID-19. Rapid SARS-CoV-2 countermeasure development is contingent on the availability of robust, scalable, and readily deployable surrogate viral assays to screen antiviral humoral responses, define correlates of immune protection, and down-select candidate antivirals. Here, we generate a highly infectious recombinant vesicular stomatitis virus (VSV) bearing the SARS-CoV-2 spike glycoprotein S as its sole entry glycoprotein and show that this recombinant virus, rVSV-SARS-CoV-2 S, closely resembles SARS-CoV-2 in its entry-related properties. The neutralizing activities of a large panel of COVID-19 convalescent sera can be assessed in a high-throughput fluorescent reporter assay with rVSV-SARS-CoV-2 S, and neutralization of rVSV-SARS-CoV-2 S and authentic SARS-CoV-2 by spike-specific antibodies in these antisera is highly correlated. Our findings underscore the utility of rVSV-SARS-CoV-2 S for the development of spike-specific therapeutics and for mechanistic studies of viral entry and its inhibition.

INTRODUCTION

A member of the family *Coronaviridae*, severe acute respiratory syndrome coronavirus-2 (SARS-CoV-2) is the causative agent of the ongoing coronavirus disease 2019 (COVID-19) pandemic that emerged in Wuhan City, China in late 2019 (Wu et al., 2020a). With more than 8 million confirmed cases and at least 435,000 deaths in over 216 countries, areas or territories as of June 15th, 2020, the global scale and impact of COVID-19 is unparalleled in living memory (Dong et al., 2020; World Health Organization, 2020). To date, mitigation strategies have relied largely on physical distancing and other public health measures. Although treatments with some small molecule inhibitors and with convalescent plasma have received approvals for emergency use and vaccines, antivirals, and monoclonal antibodies are being rapidly developed, no FDA-approved countermeasures are currently available.

The membrane-enveloped virions of SARS-CoV-2 are studded with homotrimers of the spike glycoprotein (S), which mediate viral entry into the host cell (Bosch et al., 2003; Walls et al., 2020; Wrapp et al., 2020). S trimers are post-translationally cleaved in the secretory pathway by the proprotein convertase furin to yield *N*– and *C*–terminal S1 and S2 subunits, respectively. S1 is organized into an *N*–terminal domain (NTD), a central receptor-binding domain (RBD), and a *C*–terminal domain (CTD). S2 bears the hallmarks of a "class I" membrane fusion subunit with an *N*–terminal hydrophobic fusion peptide, *N*– and *C*–terminal heptad repeat sequences, a transmembrane domain, and a cytoplasmic tail (Walls et al., 2020; Wrapp et al., 2020).

The S1 RBD engages the viral receptor, human angiotensin-converting enzyme 2 (hACE2), at the host cell surface (Hoffmann et al., 2020a; Wang et al., 2020; Zhou et al., 2020). Receptor binding is proposed to prime further S protein cleavage at the S2′ site by the transmembrane protease serine protease-2 (TMPRSS2) at the cell surface and/or by host cysteine cathepsin(s) in endosomes. S2′ cleavage activates S2 conformational rearrangements that catalyze the fusion of viral and cellular

membranes and escape of the viral genome into the cytoplasm (Hoffmann et al., 2020a).

The S glycoprotein is the major antigenic target on the virus for protective antibodies (Rogers et al., 2020; Wec et al., 2020; Wu et al., 2020a), and is thus of high significance for the development of vaccines and therapeutic antibodies. Plasma derived from COVID-19 human convalescents and replete with such antibodies has shown early promise as a COVID-19 treatment; it is currently being evaluated in clinical trials of antiviral prophylaxis and therapy (Casadevall and Pirofski, 2020). Considerable efforts are also being aimed at the identification and deployment of S-glycoprotein-specific neutralizing monoclonal antibodies (mAbs) (Cao et al., 2020; Pinto et al., 2020; Rogers et al., 2020; Wec et al., 2020; Wu et al., 2020b; Zost et al., 2020). A key requirement for the rapid development of such vaccines and treatments with convalescent plasma, small-molecule inhibitors, and recombinant biologics is the availability of safe, robust, and faithful platforms to study S-glycoprotein inhibition with high assay throughput. Given the limited access to biosafety level 3 (BSL-3) containment facilities required to safely handle SARS-CoV-2, researchers have turned to surrogate viral systems that afford studies of cell entry at biosafety level 2 (BSL-2) and facilitate rapid inhibitor screening through the use of fluorescence- or luminescence-based reporters. These include retroviruses, lentiviruses, or vesiculoviruses "pseudotyped" with SARS-CoV-2 S and competent for a single round of viral entry and infection (Lei et al., 2020; Nie et al., 2020; Ou et al., 2020; Pu et al., 2020; Tan et al., 2020; Xiong et al., 2020). However, these single-cycle, pseudotyped viruses are typically laborious to produce and challenging to scale up, yield poorly infectious preparations, and suffer background issues in some cases due to contamination with viral particles bearing the orthologous entry glycoprotein (e.g., low levels of vesicular stomatitis virus [VSV] pseudotypes bearing VSV G).

In contrast to the single-cycle pseudotypes, replication-competent recombinant VSVs (rVSVs) encoding the heterologous virus entry glycoprotein gene(s) *in cis* as their only entry protein(s) are easier to produce at high yields and also afford forward-genetic studies of viral entry. We and others have generated and used such rVSVs to safely and effectively study entry by lethal viruses that require high biocontainment (Caì et al., 2019; Jae et al., 2013; Jangra et al., 2018; Kleinfelter et al., 2015; Maier et al., 2016; Raaben et al., 2017; Whelan et al., 1995; Wong et al., 2010) Although rVSVs bearing the S glycoprotein from SARS-CoV (Fukushi et al., 2006; Kapadia et al., 2005, 2008) and the Middle East respiratory syndrome coronavirus (MERS-CoV) (Liu et al., 2018) have been developed, no such systems have been described to date for SARS-CoV-2.

Here, we generate a rVSV encoding SARS-CoV-2 S and identify key passage-acquired mutations in the S glycoprotein that facilitate robust rVSV replication. We show that the entry-related properties of rVSV-SARS-CoV-2 S closely resemble those of the authentic agent and use a large panel of COVID-19 convalescent sera to demonstrate that the neutralization of the rVSV and authentic SARS-CoV-2 by spike-specific antibodies is highly correlated. Our findings underscore the utility of rVSV-SARS-CoV-2 S for the development of spike-specific antivirals and for mechanistic studies of viral entry and its inhibition.

RESULTS

Identification of S Gene Mutations That Facilitate Robust rVSV-SARS-CoV-2 S Replication

To generate a replication-competent rVSV expressing SARS-CoV-2 S, we replaced the open-reading frame of the native VSV entry glycoprotein gene, *G*, with that of the SARS-CoV-2 *S* (Wuhan-Hu-1 isolate) (Figure 1A). We also introduced a sequence encoding the enhanced green fluorescent protein (eGFP) as an independent transcriptional unit at the first position of the VSV genome. Plasmid-based rescue of rVSV-SARS-CoV-2 S generated a slowly replicating virus bearing the wild-type S sequence. Five serial passages yielded viral populations that displayed enhanced spread. This was associated with a dramatic increase in the formation of syncytia (Figures 1B and S1) driven by S-mediated membrane fusion (Figure S1). Sequencing of this viral population identified nonsense mutations that introduced stop codons in the *S* glycoprotein gene (amino acid position C1250* and C1253*), causing 24- and 21-amino acid deletions, respectively, in the S cytoplasmic tail. SΔ24 and SΔ21 were maintained in the viral populations upon further passage and SΔ21 in all plaque-purified isolates, highlighting their likely importance as adaptations for viral growth. Viral population sequencing after four more passages identified two additional mutations—L517S and P812R in S1 and S2, respectively—whose emergence coincided with more rapid viral spread and the appearance of non-syncytium-forming infectious centers (Figure 1B, passage 5). Pelleted viral particles from clarified infected-cell supernatants incorporated the S glycoprotein, as determined by an S-specific ELISA (Figure 1C).

We next sequenced six plaque-purified viral isolates derived from the passage 9 (P9) population. All of these viral clones bore the SΔ21 deletion in the S cytoplasmic tail and spread without much syncytia formation (Figure 1D). Interestingly, all of these isolates contained three amino acid changes at S-glycoprotein positions other than 517 or 812—W64R, G261R, and A372T—in addition to the *C*–terminal SΔ21 deletion (Table S1 and Figure S2). Five of the six isolates also contained mutations H655Y or R685G. Importantly, peak titers of all these viral isolates ranged between $1-3 \times 10^7$ infectious units per mL (Figure 1E), suggesting that the mutations they share (or a subset of these mutations) drive rVSV-SARS-CoV-2 S adaptation for efficient spread in tissue culture with little or no syncytium formation.

rVSV-SARS-CoV-2 S Entry Is Cysteine Cathepsin Dependent

SARS-CoV-2 entry in cells has been shown to be dependent on the proteolytic activity of acid-dependent endosomal cysteine cathepsins, including cathepsin L (Hoffmann et al., 2020a; Wang et al., 2020). Accordingly, we tested the effects of chemical inhibitors of cysteine cathepsins on rVSV-SARS-CoV-2 S infection. Pretreatment of cells with NH_4Cl, an inhibitor of endosomal acidification, reduced entry by rVSVs bearing SARS-CoV-2 S or the Ebola virus glycoprotein (EBOV GP) in a dose-dependent manner (Figure 2A). However, S-mediated entry was comparatively less sensitive to NH_4Cl than entry by EBOV GP (Figure 2A). Next, we tested cysteine cathepsin inhibitors E-64 (Figure 2B) and FYdmk (Figure 2C). Pre-treatment of cells with
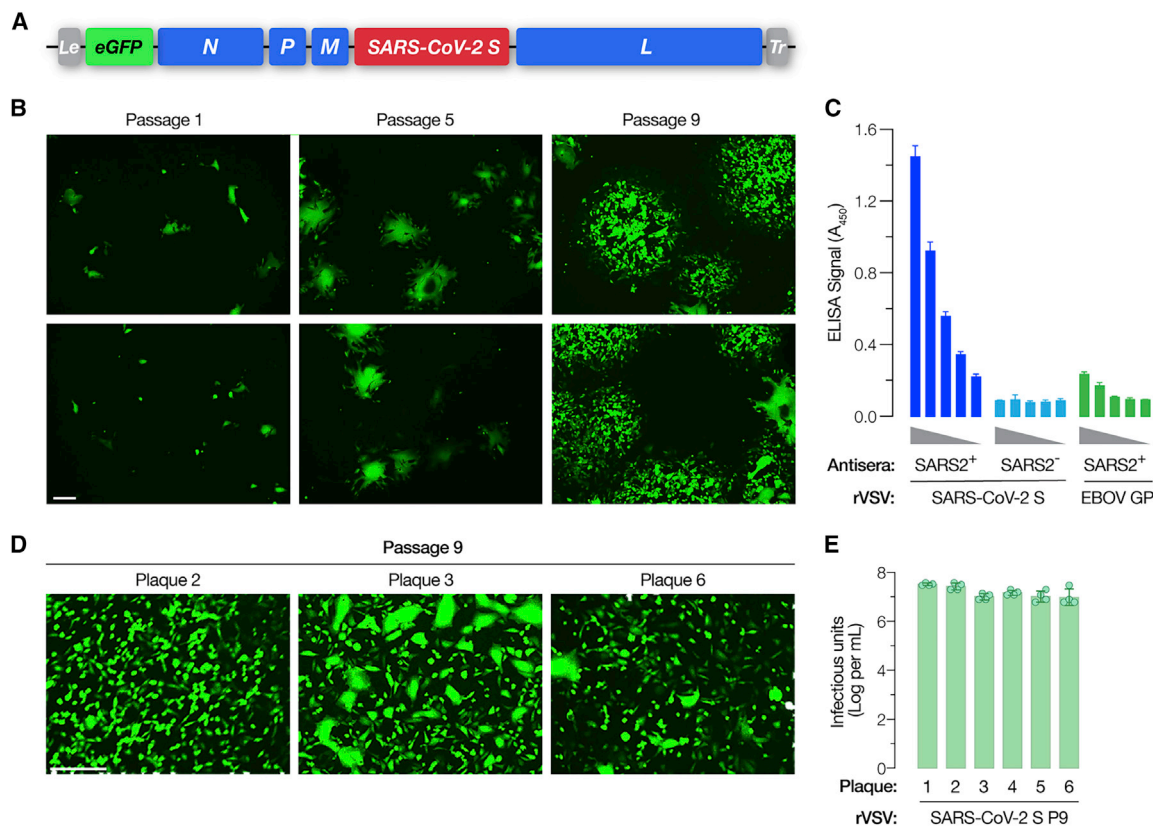
Figure 1. Generation of a Recombinant Vesicular Stomatitis Virus (rVSV) Bearing the SARS-CoV-2 Spike (S) Glycoprotein
(A) Schematic representation of the VSV genome in which its native glycoprotein gene has been replaced by that encoding the SARS-CoV-2 S protein. The VSV genome has been further modified to encode an enhanced green fluorescent protein (eGFP) reporter to easily score for infection.
(B) Infectious center formation assay on Vero cells at 24 h post-infection showing growth of the rVSV-SARS-CoV-2 S after the indicated number of rounds of serial passage of the passage #1 virus (carrying wild-type [WT] S sequences) on Huh7.5.1 cell line (scale bar, 100 μm). Two representative images for each virus passage, showing infected cells pseudo-colored in green, from one of the two independent experiments are shown here.
(C) Incorporation of SARS-CoV-2 S into rVSV particles captured on an ELISA plate was detected using antiserum from a COVID-19 convalescent donor (average ± SD, n = 12 from 3–4 independent experiments). Serum from a COVID-19-negative donor and rVSVs bearing Ebola virus glycoprotein (EBOV GP) were used as negative controls (average ± SD, n = 6 from 2 independent experiments).
(D) Representative images showing Vero cells infected with plaque #2, #3, and #6 viruses at 16 h post-infection (scale bar, 100 μm).
(E) Production of infectious virions at 48 h post-infection from Vero cells infected with the indicated plaque-purified viruses. Titers were measured on Vero cells overexpressing TMPRSS2 (n = 4, from two independent titrations).

both of these compounds also inhibited S-mediated entry, albeit with reduced sensitivity relative to that observed for EBOV GP-dependent entry (Figures 2B and 2C). Together, these findings confirm that rVSV-SARS-CoV-2 S resembles the authentic agent in its requirements for endosomal acid pH and cysteine cathepsins. They also suggest a reduced dependence on these host factors for entry by SARS-CoV-2 S relative to EBOV GP, a model glycoprotein known to fuse in late endo/lysosomal compartments following extensive endosomal proteolytic processing.

TMPRSS2 Can Mediate rVSV-SARS-CoV-2 S Entry
The Type II transmembrane serine protease TMPRSS2 plays a key role in the infection and spread of a number of enveloped viruses in cells of the human airway (Choi et al., 2009; Shen et al., 2017). TMPRSS2 cleavage of the hemagglutinin spike precursors (HA0) of some influenza A and B viruses at a monobasic site generates HA1 and HA2 subunits, thereby priming HA for

viral membrane fusion (Böttcher-Friebertshäuser et al., 2014; Limburg et al., 2019; Böttcher-Friebertshäuser et al., 2010; Chaipan et al., 2009). TMPRSS2 can also activate membrane fusion by the spike glycoproteins of human coronaviruses, including those of SARS-CoV and MERS-CoV, by cleaving the spike at the monobasic S2′ site during entry (Kawase et al., 2012; Zhou et al., 2015). Recent work indicates that TMPRSS2 may play a similar role in SARS-CoV-2 entry into human airway and intestinal cells (Bestle et al., 2020; Zang et al., 2020; Hoffmann et al., 2020b). Accordingly, we evaluated the effect of the trypsin-like serine protease inhibitor camostat mesylate (camostat), previously shown to block TMPRSS2 catalytic activity and inhibit viral glycoprotein activation (Zhou et al., 2015; Kawase et al., 2012; Nimishakavi et al., 2015), on rVSV-SARS-CoV-2 S infection. Pretreatment of Vero grivet monkey cells with camostat had little effect, consistent with their low expression levels of TMPRSS2 (Hoffmann et al., 2020b). By contrast, camostat treatment
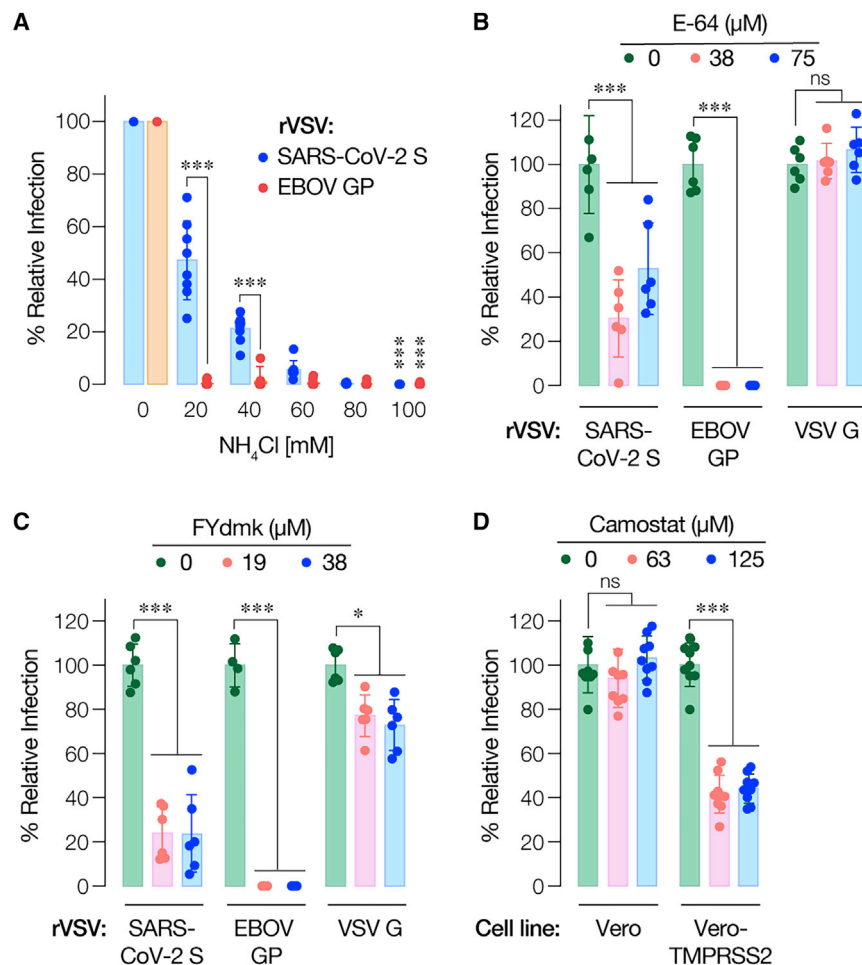
Figure 2. rVSV-SARS-CoV-2 S Infection Requires the Activity of Cysteine Cathepsin Proteases

(A) Huh7.5.1 cells pre-treated for 1 h at 37°C with the indicated concentrations of NH_4Cl were infected with pre-titrated amounts of rVSVs bearing SARS-CoV-2 S or EBOV GP. Infection was scored by eGFP expression at 16–18 h post-infection (average ± SD, n = 8 from 2 independent experiments).

(B) Vero cells pre-treated for 90 min at 37°C with the indicated concentrations of pan-cysteine cathepsin inhibitor E-64 were infected with pre-titrated amounts of rVSVs bearing SARS-CoV-2 S, EBOV GP, or VSV G and scored for infection as above (average ± SD, n = 6 from 3 independent experiments, except n = 4 from 2 independent experiments for EBOV GP).

(C) Vero cells pre-treated for 90 min at 37°C with the indicated concentrations of cathepsin L/B inhibitor FYdmk were infected with pre-titrated amounts of rVSVs bearing SARS-CoV-2 S, EBOV GP, or VSV G. Infection was scored as above (average ± SD, n = 6 from 3 independent experiments).

(D) Vero cells and Vero cells overexpressing TMPRSS2 pre-treated for 120min at 37C with the indicated concentrations of camostat]were infected with pre-titrated amounts of rVSVs bearing SARS-CoV-2 S and subsequently scored for infection. In panels (B)–(D), all comparisons were made between vehicle- and inhibitor-treated samples. ns,not statistically significant. *p < 0.033, ***p < 0.001.

significantly reduced VSV-SARS-CoV-2 S infection in Vero cells transduced to express human TMPRSS2 (Vero-TMPRSS2), as reported previously (Hoffmann et al., 2020a; Figure 2D). These findings suggest that TMPRSS2 can promote cell entry by rVSV-SARS-CoV-2 S.

Human ACE2 Is Required for rVSV-SARS-CoV-2 S Entry

SARS-CoV-2 uses hACE2 as its entry receptor (Letko et al., 2020; Shang et al., 2020b, 2020a). Baby hamster kidney (BHK21) cells do not express detectable levels of ACE2 protein and are resistant to SARS-CoV-2 entry (Chu et al., 2020; Hoffmann et al., 2020a; Wang et al., 2020). Concordantly, we observed no detectable infection by rVSV-SARS-CoV-2 S in BHK-21 cells (Figure 3A, top left). By contrast, BHK21 cells transduced to express hACE2 (Figure 3A, top right) were highly susceptible to rVSV-SARS-CoV-2 S (Figure 3A, bottom right and Figure 3B).

To directly establish an entry-relevant interaction between rVSV-SARS-CoV-2 S and hACE2, we expressed and purified the spike RBD (Figure 3C) and pre-incubated it with target cells. RBD pre-treatment inhibited rVSV-SARS-CoV-2 S entry in a specific and dose-dependent manner (Figure 3D). Moreover, pre-incubation of cells with an hACE2-specific mAb, but not an

isotype-matched control mAb, potently abolished rVSV-SARS-CoV-2 S entry (Figure 3E). These findings provide evidence that rVSV-SARS-CoV-2 S entry and infection, like that of the authentic agent, requires spike RBD-hACE2 engagement.

rVSV-SARS-CoV-2 S Infects Cells of Human Airway Origin in an ACE2-Dependent Manner

SARS-CoV-2 can infect multiple cell types in the human airway, including ciliated epithelial cells of the bronchial and bronchiolar mucosae and type I and II pneumocytes of the lung (Rockx et al., 2020; Hui et al., 2020). We assessed rVSV-SARS-CoV-2 entry and infection in epithelial cell lines that serve as models of human respiratory function. Specifically, we found that the human lung adenocarcinoma cell line Calu3 was highly susceptible to infection (Figure 4A) in a manner that was sensitive to treatment with a hACE2-specific mAb (Figures 4B and 4C). By contrast, the human lung adenocarcinoma cell line A549 was refractory to infection (Figure 4D), as previously documented with authentic SARS-CoV-2 and a single-cycle VSV vector bearing SARS-CoV-2 S (Chu et al., 2020; Harcourt et al., 2020; Hoffmann et al., 2020a; Hui et al., 2020). Because poorly differentiated A549 cells express little ACE2 (Jia et al., 2005; Mossel et al., 2005; Figure 4E), we transduced these cells to express hACE2 and then exposed
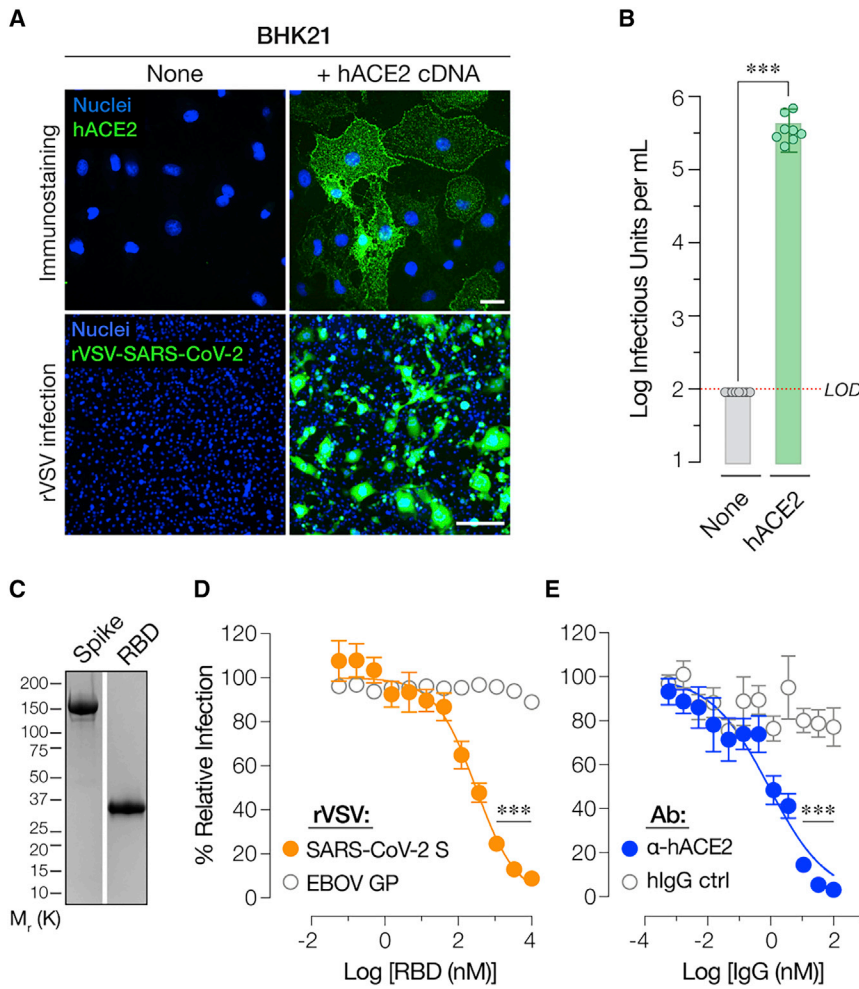
Figure 3. rVSV-SARS-CoV-2 S Infection Requires Human ACE2

(A) Naïve (None) baby hamster kidney (BHK21) cells or cells transduced with a retrovirus carrying human ACE2 cDNA (+ hACE2 cDNA) were immunostained for hACE2 expression using an anti-ACE2 antibody. Cells were imaged by fluorescence microscopy. The hACE2 signal is pseudo-colored green (top panel, scale bar = 20 μm). These cells were also exposed to serial 5-fold dilutions of rVSV-SARS-CoV-2 S and infection was scored by eGFP expression (bottom panel, scale bar = 50 μm). Representative images from one of 3 independent experiments are shown.

(B) Enumeration of eGFP-positive green cells (Average ± SD, n = 8 from 3 independent experiments). Red dotted line indicates the assay limit of detection (LOD).

(C) Recombinant, Ni-NTA–affinity purified S1-S2 ectodomain (Spike) or the receptor binding domain (RBD) of the SARS-CoV-2 S protein were subjected to SDS-PAGE and Coomassie staining. A representative image from one of two independent purification trials is shown here.

(D) Monolayers of Huh7.5.1 cells were pre-incubated with serial 3-fold dilutions of the purified RBD for 1 h at 37°C and then infected with pre-titrated amounts of rVSVs bearing SARS-CoV-2 S or EBOV GP. At 16–18 h post-infection, cells were fixed, nuclei counter-stained with Hoechst-33342, and infection (eGFP expression) was scored by fluorescence microscopy. It is represented as % relative infection (no RBD = 100%, Average ± SEM, n = 8 from 3–4 [rVSV-SARS-CoV-2 S] or n = 4 from 2 [rVSV-EBOV GP] independent experiments).

(E) Monolayers of Huh7.5.1 cells pre-incubated for 1 h at 37°C with 3-fold serial dilutions of anti-human ACE2 antibody or negative control (hIgG) were infected with pre-titrated amounts of rVSV-SARS-CoV-2 S. Infection was scored as above and is represented as % relative infection (no antibody = 100%, Average ± SD, n = 8 from 3–4 independent experiments). ***p < 0.001.

---

them to virus. The A549-hACE2 cells were more susceptible than their parental cells by a factor of ≈10⁴ (Figure 4E). Thus, rVSV-SARS-CoV-2 S can enter and infect cells of human airway origin in an ACE2-dependent fashion.
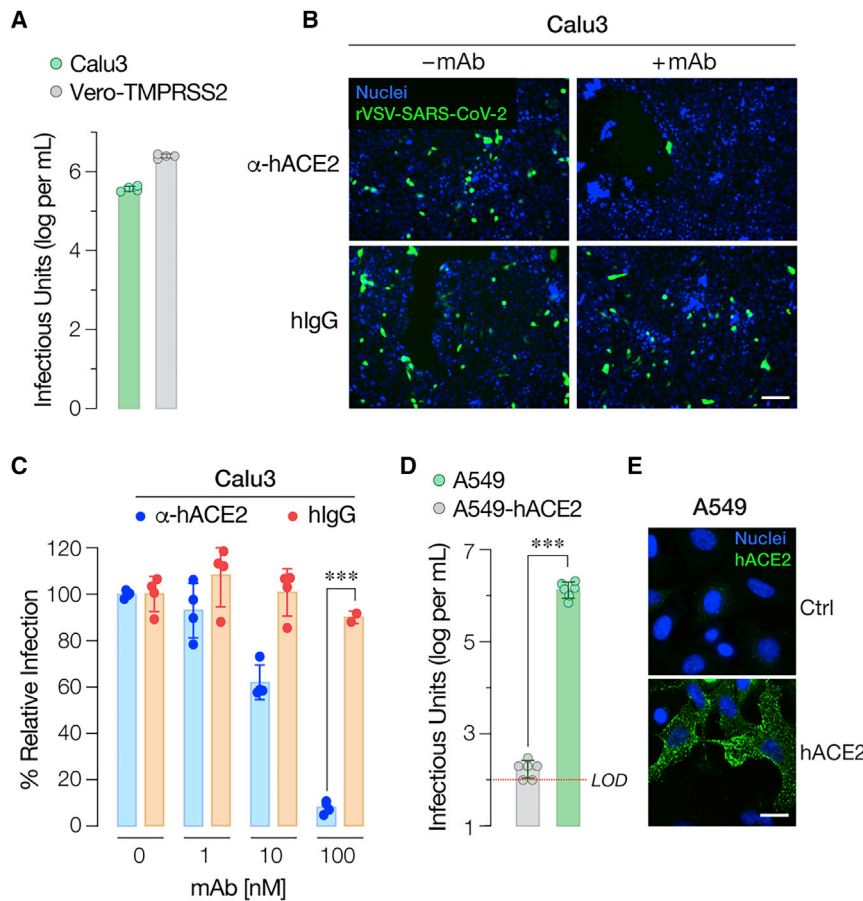
S-Protein-Targeting Antibodies in COVID-19 Convalescent Sera Specifically Account for rVSV-SARS-CoV-2 S Neutralization

Prior to examining the performance of rVSV-SARS-CoV-2 S in neutralization assays with human antisera, we sought to establish a specific role for interaction between anti-spike antibodies in these sera and the VSV-borne S protein. Accordingly, we first evaluated the reactivity of two sera with rVSV-neutralizing activity (Figure S3) against viral particles by ELISA. Both sera specifically recognized rVSV-SARS-CoV-2 S particles (Figure 5A) and were also shown to be reactive against a purified, trimeric preparation of the spike glycoprotein (Wrapp et al., 2020; R.H.B., unpublished data). Further, serial pre-incubation of each serum

with purified S immobilized on a high-binding plate depleted its capacity to inhibit rVSV-SARS-CoV-2 S infection to a degree that was commensurate with its content of S-specific antibodies (Figures 5B and 5C). By contrast, parallel pre-incubations with blocked plates had little or no effect (Figure 5C). These results indicate that S-glycoprotein-targeting antibodies in COVID-19 convalescent sera specifically mediate rVSV-SARS-CoV-2 S neutralization.

The Susceptibilities of rVSV-SARS-CoV-2 S and Authentic SARS-CoV-2 to Antibody-Mediated Neutralization Are Highly Correlated

We compared the capacities of human antisera derived from 40 COVID-19 convalescent donors to block infection by rVSV-SARS-CoV-2 S and authentic SARS-CoV-2 in a microneutralization format. Briefly, pre-titrated amounts of viral particles were incubated with serial dilutions of each antiserum, and target cells were then exposed to the virus-antiserum mixtures. Viral

infection was determined by enumerating eGFP-positive cells (rVSV) as above (Figure 1) or cells immunoreactive with a SARS-CoV-2 nucleocapsid protein-specific antibody (authentic virus) (Figure 6A). Heatmaps of viral infectivity revealed similar antiserum donor- and dose-dependent neutralization patterns for rVSV-SARS-CoV-2 S and authentic SARS-CoV-2 (Figure 6B). Comparison of the serum dilutions at half-maximal neutralization derived from logistic curve fits (neutralization IC_{50}) revealed a 3-to10-fold shift toward enhanced neutralization with rVSV-SARS-CoV-2 S (Figure 6C). The origin of this difference is unclear but does not appear to arise from viral-passage-dependent changes in the rVSV-encoded spike gene sequence (Figure S4). Rather, it may reflect assay-specific differences in the rVSV and authentic virus microneutralization formats employed herein. Nevertheless, the relative potencies of the antisera against rVSV-SARS-CoV-2 S and authentic SARS-CoV-2 were well correlated (R^2 = 0.76) (Figure 6D). In sum, these findings demonstrate the suitability of rVSV-SARS-CoV-2 S for rapid, high-throughout, reporter-based assays of spike-glycoprotein-dependent entry and its inhibition.

DISCUSSION

There is an urgent need for vaccines and therapeutics to prevent and treat COVID-19. The rapid development of SARS-CoV-2 countermeasures is contingent on the availability of robust, scalable, and readily deployable surrogate viral systems to screen antiviral humoral responses and define correlates of immune protection. Such tools would also facilitate the efficient down-selection of candidate antivirals and studies of their mechanisms of action. Here, we describe a highly infectious recombinant vesicular stomatitis virus bearing the SARS-CoV-2 spike glycoprotein S that closely resembles the authentic agent in its entry-related properties. We show that rVSV-SARS-CoV-2 S affords the high-throughput, reporter-based screening of small-molecule and antibody-based inhibitors targeting the viral spike glycoprotein with performance characteristics comparable to those of SARS-CoV-2.

rVSV-SARS-CoV-2 S initially replicated poorly in cell culture following its rescue from plasmids, but we noted accelerated viral growth at passage 5 (Figure 1). This coincided with the emergence of viral variants bearing S glycoproteins with 21- or 24-amino-acid truncations of their cytoplasmic tails, as also observed by Case and co-workers (Case et al., 2020). The cytoplasmic tails of the S glycoproteins of SARS-CoV and SARS-CoV-2 are highly similar and carry signals for their retention in the endoplasmic reticulum (ER), including a conserved Kx Hxx motif located near the C–terminus (McBride et al., 2007; Ujike et al., 2016). 18- to 19-amino-acid deletions in the cytoplasmic tails of SARS-CoV S (Fukushi et al., 2006; Fukushi et al., 2005) and SARS-CoV-2 S (Ou et al., 2020) have been shown to increase the infectivity of single-cycle VSV-S pseudotypes. As previously observed for ER/Golgi-localizing hantavirus
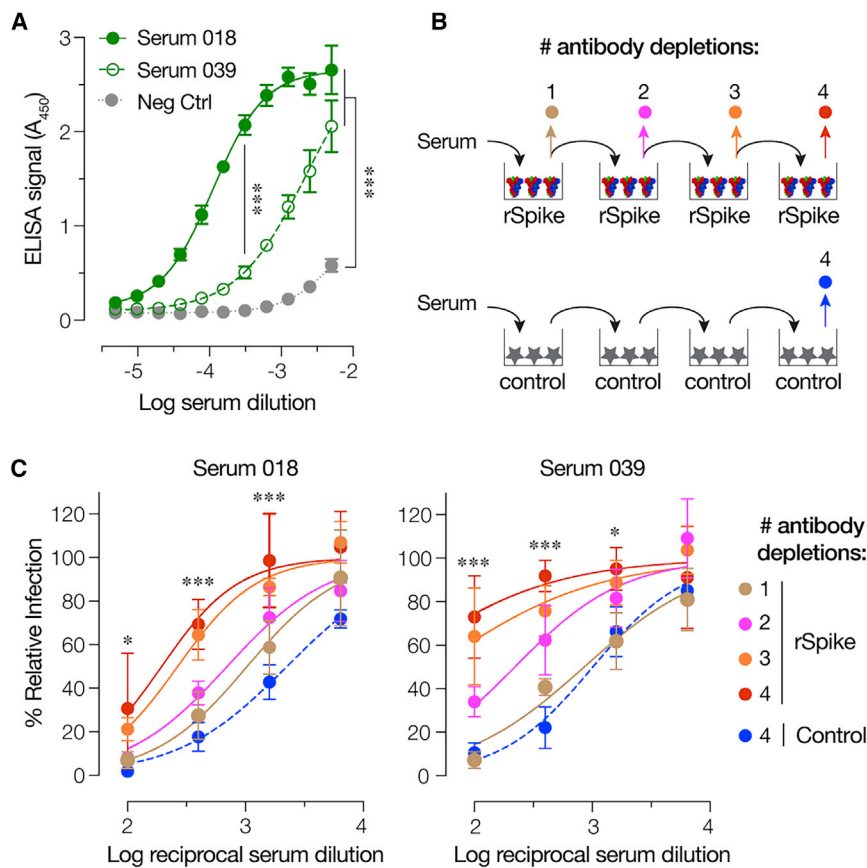
Figure 5. rVSV-SARS-CoV-2 S Neutralization Is Mediated by S-Glycoprotein-Targeting Antibodies in Human Antisera

(A) ELISA plates coated with rVSV-SARS-CoV-2 S were incubated with serial 2-fold dilutions of serum 18, serum 39, or negative control serum. Bound S-specific antibodies were detected with an anti-human HRP-conjugated secondary antibody (average ± SD, n = 4 from 2 independent experiments).

(B) Schematic of the antibody depletion study.

(C) Pre-titrated amounts of serum 18 and serum 39 were sequentially incubated with SARS-CoV-2 S-coated high-binding plates to deplete S-specific antibodies. Capacity of the depleted sera (and control sera incubated with only the blocking agent) to neutralize rVSV-SARS-CoV-2 S was then estimated by incubating pre-titrated amounts of rVSV at the indicated dilutions of sera at 37°C for 1 h prior to infecting monolayers of Huh7.5.1 cells. Cells were scored for infection as above (average ± SD, n = 4 from 2 independent experiments). In panels (A), (C), and (D), p values for pairwise comparisons of the untreated sample and inhibitor-treated sample means are shown, unless otherwise indicated. In panels (C) and (D), the depletion #4 and depletion control were compared. *p < 0.033, ***p < 0.001.

glycoproteins (Slough et al., 2019), these deletions likely redistribute S glycoproteins to the cell surface, thereby relieving the spatial mismatch in budding between VSV and SARS-CoV2 (plasma membrane versus ER, respectively) and enhancing S incorporation into VSV particles.

Accelerated growth by rVSV-SARS-CoV-2 S around passage 5 was accompanied by a marked increase in the occurrence of syncytia (see Figure 1B) due to S-mediated cell-cell fusion (Figure S1). This may reflect a functional property of the cytoplasmic-tail-deleted S variants, including perturbations in their subcellular localization, as discussed above. Strikingly, passage 9 stocks and highly infectious viral plaque isolates from these stocks displayed a pattern of spreading infection more typical for rVSVs, with few large syncytia in evidence (Figure 1B). In this regard, it is tempting to speculate that one or more additional S glycoprotein mutations detected in the passage 5–9 viral populations and in the six plaque isolates (Table S1) arose as compensatory changes to suppress the syncytiogenic propensity of the rVSV-encoded SΔ21 glycoprotein spikes. Indeed, several mutations in the S1 NTD and RBD may serve to modulate spike glycoprotein fusogenicity, as also may mutations near or at the S1–S2 cleavage site (H655Y and R685G, respectively) and/or at the S2′ cleavage site (P812R) (Table S1 and Figure S2). Further, at least one mutation (H655Y), present in five of six rVSV-SARS-CoV-2 S plaque isolates, has arisen during natural SARS-CoV-2 evolution in humans (Yang et al., 2020), during transmission studies in a hamster model (Chan et al., 2020), and possibly dur-

ing SARS-CoV-2 passage in tissue culture (this report). Our current efforts are aimed at understanding what role(s) these mutations in the S glycoprotein ectodomain play in the maintenance of high levels of rVSV infectivity without the formation of large numbers of syncytia. These findings also highlight a feature of rVSV-SARS-CoV-2 S not shared by any of the viral entry surrogates described to date: its utility for forward genetics. This can be used to dissect structure-function relationships in the SARS-CoV-2 spike glycoprotein and to elucidate the mechanisms of action of spike- or entry-targeted antivirals.

We demonstrate that rVSV-SARS-CoV-2 S can be used to rapidly and faithfully assess the neutralizing activities of large panels of COVID-19 convalescent sera (this report, Figure 6) and spike-directed mAbs (Wec et al., 2020). We have exploited the fidelity and high throughput of our rVSV-based 384-well plate microneutralization assay to rapidly pre-screen >300 COVID-19 convalescents and identify potential convalescent plasma donors first for the expanded access program and now for an ongoing randomized controlled trial of convalescent plasma therapy (Casadevall and Pirofski, 2020; NYU Langone Health/Albert Einstein College of Medicine, 2020; K.C. and L.-a.P., unpublished data). The utility and reliability of this approach is further enhanced by its synergy with the new SARS-CoV-2 microneutralization assay also described herein (Figures 6A and 6B), which provides a rapid and non-subjective alternative to classical PRNT assays. When used in combination, these assays should afford the rapid mechanistic interrogation of cellular factors and antivirals that act at any step of the viral multiplication cycle—entry hits should affect both the rVSV and the authentic virus, whereas post-entry hits should affect only the latter.
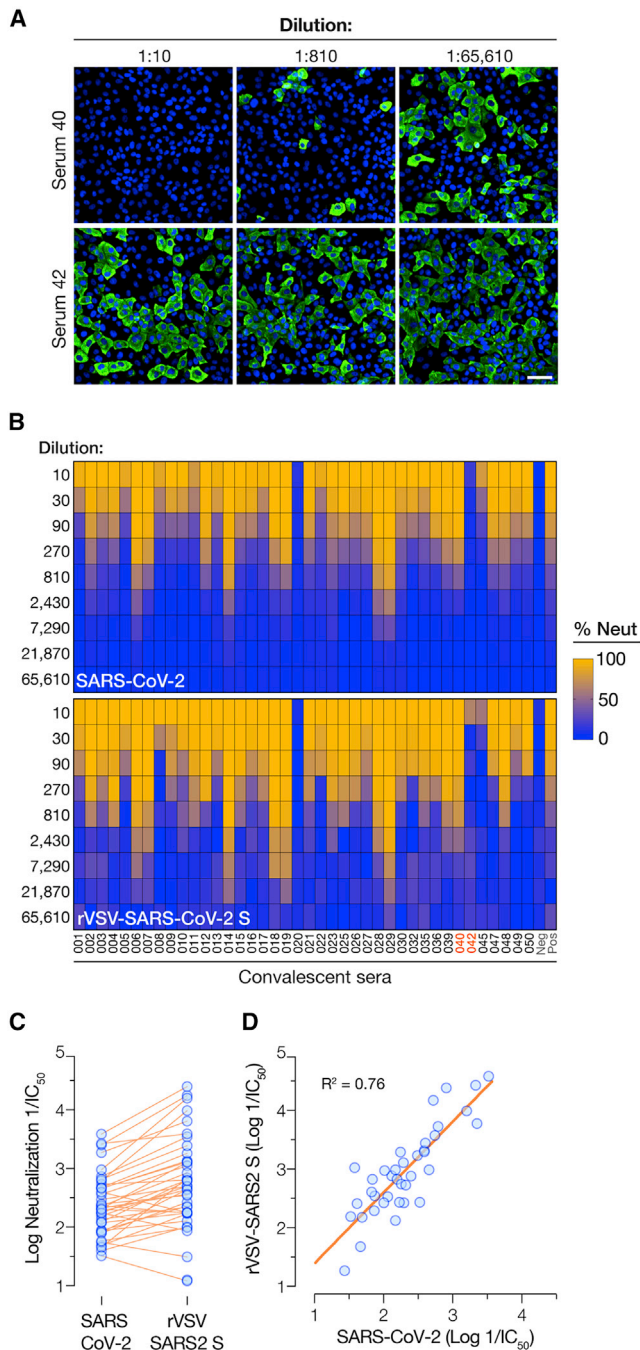
Figure 6. Correlation of Convalescent Serum-Mediated Neutralization of rVSV-SARS-CoV-2 S and Authentic SARS-CoV-2

(A) Pre-titrated amounts of SARS-CoV-2 were incubated with serial 3-fold dilutions of antisera from COVID-19 convalescent donors or negative control at 37°C for 1 h. Virus-serum mixtures were then applied to monolayers of Vero-E6 cells. At 24 h post-infection, cells were fixed, permeabilized and immuno-stained with a SARS-CoV nucleocapsid-specific antibody. Nuclei were counterstained, and infected cells were scored for the presence of nucleo-capsid antigen. Representative images from one of the 2 independent experiments are shown (scale bar, 200 μm).

(B) Pre-titrated amounts of rVSV-SARS-CoV-2 S were incubated with serial 3-fold dilutions of antisera from COVID-19 convalescent patients or negative control at 37°C for 1 h. Virus:serum mixtures were then applied to monolayers

As the COVID-19 pandemic continues apace and the development of plasma-, hyperimmune globulin-, mAb-, and small-molecule-based countermeasures accelerates, the need for highly scalable viral assays continues to mount. The availability of highly infectious rVSV surrogates that can be scaled up with relative ease for antiviral screening and readily deployed in reporter-based microneutralization assays will facilitate these efforts.

Limitations of Study

rVSV-SARS-CoV-2 S has only been tested in cell culture. Thus, we cannot conclusively rule out that it may not be well tolerated *in vivo*. Given this theoretical safety concern, lab workers should exercise due caution in handling an agent that is potentially infectious in humans. Until the safety of rVSV-SARS-CoV-2 S has been evaluated and established in appropriate animal model(s), we will only distribute it to researchers for *in vitro* work to be performed at biosafety level 2 or higher, as approved by their institutional biosafety committee.

STAR★METHODS

Detailed methods are provided in the online version of this paper and include the following:

- KEY RESOURCES TABLE
- RESOURCE AVAILABILITY
  - ○ Lead Contact
  - ○ Materials Availability
  - ○ Data and Code Availability
- EXPERIMENTAL MODEL AND SUBJECT DETAILS
  - ○ Cells
  - ○ Generation of Cells Overexpressing hACE2 or TMPRSS2
  - ○ Convalescent Serum Samples
  - ○ Generation of rVSV-SARS-CoV-2
  - ○ SARS-CoV-2 Stock Preparation
  - ○ SARS-CoV2 Spike Glycoprotein RBD Expression and Purification
  - ○ SARS-CoV2 Spike Glycoprotein Expression and Purification
- METHOD DETAILS
  - ○ Detection of S Protein in rVSV-SARS-CoV-2
  - ○ NH_4Cl Inhibition Experiments
  - ○ Cathepsin Inhibitor Experiments
  - ○ TMPRSS2 Inhibitor Experiments
  - ○ Detection of hACE2 in BHK21 and A549 Transfected Cells
  - ○ rVSV-SARS-CoV-2 S Microneutralization Assay

of Vero cells. At 7 h post-infection, cells were fixed, nuclei were counterstained, and infected cells were scored by GFP expression. Heatmaps showing % neutralization of authentic SARS-CoV-2 or rVSV-SARS-CoV-2 S by the panel of 40 antisera are shown (Averages of n = 4 from 2 independent experiments).

(C and D) Comparison of the neutralizing activities of the antisera (log reciprocal IC_{50} values) against authentic SARS-CoV-2 and rVSV-SARS-CoV-2 S ("rVSV SARS2 S"). (D) Linear regression analyses of neutralization IC_{50} values from panel C.

- ○ Anti-hACE2 Antibody Blocking Assay
- ○ RBD Competition Assay
- ○ S-Mediated Antibody Depletion Assay
- ○ SARS-CoV-2 Neutralization Assay
- ○ Syncytia Inhibition Assay
- ● QUANTIFICATION AND STATISTICAL ANALYSIS

SUPPLEMENTAL INFORMATION

Supplemental Information can be found online at https://doi.org/10.1016/j.chom.2020.06.020.

AUTHOR CONTRIBUTIONS

Conceptualization, M.E.D., D.H., K.C., R.K.J. ; Methodology, M.E.D., D.H., J.M.D., A.S.H., K.C., R.K.J.; Investigation, M.E.D., D.H., R.H.B., G.L., O.V., S.A.A., A.S.H., R.K.J.; Resources, M.E.D., D.H., R.H.B., A.S.W., O.V., J.M.F., E.L., C.F., R.J.M., G.G., L.-a.P., J.P.D., J.M.D., J.R.L., K.C., R.K.J.; Data Curation, M.E.D., D.H., R.H.B., A.S.W., E.L., C.F., A.M., D.K., J.Q., K.C., R.K.J.; Writing—Original Draft, M.E.D., D.H., A.S.H., K.C., R.K.J.; Writing—Review & Editing, all authors; Visualization, M.E.D., D.H., R.H.B., G.L., K.C., R.K.J.; Supervision, L.-a.P., J.P.D., J.M.D., J.R.L., A.S.H., K.C., R.K.J.; Project administration, K.C., R.K.J.; Funding Acquisition, J.B., L.-a.P., J.P.D., J.M.D., J.R.L., K.C.

REFERENCES

Amanat, F., Stadlbauer, D., Strohmeier, S., Nguyen, T.H.O., Chromikova, V., McMahon, M., Jiang, K., Arunkumar, G.A., Jurczyszak, D., Polanco, J., et al. (2020). A serological assay to detect SARS-CoV-2 seroconversion in humans. Nat. Med. https://doi.org/10.1038/s41591-020-0913-5.

Bestle, D., Heindl, M.R., Limburg, H., Van Lam van, T., Pilgram, O., Moulton, H., Stein, D.A., Hardes, K., Eickmann, M., Dolnik, O., et al. (2020). TMPRSS2 and furin are both essential for proteolytic activation and spread of SARS-CoV-2 in human airway epithelial cells and provide promising drug targets. bioRxiv. https://doi.org/10.1101/2020.04.15.042085.

Bosch, B.J., van der Zee, R., de Haan, C.A.M., and Rottier, P.J.M. (2003). The coronavirus spike protein is a class I virus fusion protein: structural and functional characterization of the fusion core complex. J. Virol. 77, 8801–8811.

Böttcher-Friebertshäuser, E., Freuer, C., Sielaff, F., Schmidt, S., Eickmann, M., Uhlendorff, J., Steinmetzer, T., Klenk, H.-D., and Garten, W. (2010). Cleavage of influenza virus hemagglutinin by airway proteases TMPRSS2 and HAT differs in subcellular localization and susceptibility to protease inhibitors. J. Virol. 84, 5605–5614.

Böttcher-Friebertshäuser, E., Garten, W., Matrosovich, M., and Klenk, H.D. (2014). The hemagglutinin: a determinant of pathogenicity. Curr. Top. Microbiol. Immunol. 385, 3–34.

Caì, Y., Yú, S., Jangra, R.K., Postnikova, E.N., Wada, J., Tesh, R.B., Whelan, S.P.J., Lauck, M., Wiley, M.R., Finch, C.L., et al. (2019). Human, nonhuman primate, and bat cells are broadly susceptible to tibrovirus particle cell entry. Front. Microbiol. 10, 856.

Cao, Y., Su, B., Guo, X., Sun, W., Deng, Y., Bao, L., Zhu, Q., Zhang, X., Zheng, Y., Geng, C., et al. (2020). Potent neutralizing antibodies against SARS-CoV-2 identified by high-throughput single-cell sequencing of convalescent patients' B cells. Cell 182, 73–84.e16.

Casadevall, A., and Pirofski, L.A. (2020). The convalescent sera option for containing COVID-19. J. Clin. Invest. 130, 1545–1548.

Case, J.B., Rothlauf, P.W., Chen, R.E., Liu, Z., Zhao, H., Kim, A.S., Bloyet, L.-M., Zeng, Q., Tahan, S., et al. (2020). Neutralizing antibody and soluble ACE2 inhibition of a replication-competent VSV2 SARS-CoV-2 and a clinical isolate of SARS-CoV-2. Cell Host Microbe.

Chaipan, C., Kobasa, D., Bertram, S., Glowacka, I., Steffen, I., Tsegaye, T.S., Takeda, M., Bugge, T.H., Kim, S., Park, Y., et al. (2009). Proteolytic activation of the 1918 influenza virus hemagglutinin. J. Virol. 83, 3200–3211.

Chan, J.F.-W., Zhang, A.J., Yuan, S., Poon, V.K.-M., Chan, C.C.-S., Lee, A.C.-Y., Chan, W.-M., Fan, Z., Tsoi, H.-W., Wen, L., et al. (2020). Simulation of the clinical and pathological manifestations of Coronavirus Disease 2019 (COVID-19) in golden Syrian hamster model: implications for disease pathogenesis and transmissibility. Clin. Infect. Dis. ciaa325.

Choi, S.-Y., Bertram, S., Glowacka, I., Park, Y.W., and Pöhlmann, S. (2009). Type II transmembrane serine proteases in cancer and viral infections. Trends Mol. Med. 15, 303–312.

Chu, H., Chan, J.F.-W., Wang, Y., Yuen, T.T.-T., Chai, Y., Hou, Y., Shuai, H., Yang, D., Hu, B., Huang, X., et al. (2020). Comparative replication and immune activation profiles of SARS-CoV-2 and SARS-CoV in human lungs: an ex vivo study with implications for the pathogenesis of COVID-19. Clin. Infect. Dis. ciaa410.

Dong, E., Du, H., and Gardner, L. (2020). An interactive web-based dashboard to track COVID-19 in real time. Lancet Infect. Dis. 20, 533–534.

Fukushi, S., Mizutani, T., Saijo, M., Matsuyama, S., Miyajima, N., Taguchi, F., Itamura, S., Kurane, I., and Morikawa, S. (2005). Vesicular stomatitis virus pseudotyped with severe acute respiratory syndrome coronavirus spike protein. J. Gen. Virol. 86, 2269–2274.

Fukushi, S., Mizutani, T., Saijo, M., Kurane, I., Taguchi, F., Tashiro, M., and Morikawa, S. (2006). Evaluation of a novel vesicular stomatitis virus pseudotype-based assay for detection of neutralizing antibody responses to SARS-CoV. J. Med. Virol. 78, 1509–1512.

Harcourt, J., Tamin, A., Lu, X., Kamili, S., Sakthivel, S.K., Murray, J., Queen, K., Tao, Y., Paden, C.R., Zhang, J., et al. (2020). Severe Acute Respiratory Syndrome Coronavirus 2 From Patient With Coronavirus Disease, United States, 26, pp. 1266–1273.

Hoffmann, M., Kleine-Weber, H., Schroeder, S., Krüger, N., Herrler, T., Erichsen, S., Schiergens, T.S., Herrler, G., Wu, N.H., Nitsche, A., et al. (2020a). SARS-CoV-2 Cell Entry Depends on ACE2 and TMPRSS2 and Is Blocked by a Clinically Proven Protease Inhibitor. Cell 181, 271–280.e8.

Hoffmann, M., Kleine-Weber, H., and Pöhlmann, S. (2020b). A Multibasic Cleavage Site in the Spike Protein of SARS-CoV-2 Is Essential for Infection of Human Lung Cells. Mol. Cell 78, 779–784.e5.

Hui, K.P.Y., Cheung, M.-C., Perera, R.A.P.M., Ng, K.-C., Bui, C.H.T., Ho, J.C.W., Ng, M.M.T., Kuok, D.I.T., Shih, K.C., Tsao, S.-W., et al. (2020).

Tropism, replication competence, and innate immune responses of the coronavirus SARS-CoV-2 in human respiratory tract and conjunctiva: an analysis in ex-vivo and in-vitro cultures. Lancet Respir. Med., S2213-2600(20)30193-4.

Jae, L.T., Raaben, M., Riemersma, M., van Beusekom, E., Blomen, V.A., Velds, A., Kerkhoven, R.M., Carette, J.E., Topaloglu, H., Meinecke, P., et al. (2013). Deciphering the glycosylome of dystroglycanopathies using haploid screens for lassa virus entry. Science 340, 479–483.

Jangra, R.K., Herbert, A.S., Li, R., Jae, L.T., Kleinfelter, L.M., Slough, M.M., Barker, S.L., Guardado-Calvo, P., Román-Sosa, G., Dieterle, M.E., et al. (2018). Protocadherin-1 is essential for cell entry by New World hantaviruses. Nature 563, 559–563.

Jia, H.P., Look, D.C., Shi, L., Hickey, M., Pewe, L., Netland, J., Farzan, M., Wohlford-Lenane, C., Perlman, S., and McCray, P.B., Jr. (2005). ACE2 receptor expression and severe acute respiratory syndrome coronavirus infection depend on differentiation of human airway epithelia. J. Virol. 79, 14614–14621.

Kapadia, S.U., Rose, J.K., Lamirande, E., Vogel, L., Subbarao, K., and Roberts, A. (2005). Long-term protection from SARS coronavirus infection conferred by a single immunization with an attenuated VSV-based vaccine. Virology 340, 174–182.

Kapadia, S.U., Simon, I.D., and Rose, J.K. (2008). SARS vaccine based on a replication-defective recombinant vesicular stomatitis virus is more potent than one based on a replication-competent vector. Virology 376, 165–172.

Kawase, M., Shirato, K., van der Hoek, L., Taguchi, F., and Matsuyama, S. (2012). Simultaneous treatment of human bronchial epithelial cells with serine and cysteine protease inhibitors prevents severe acute respiratory syndrome coronavirus entry. J. Virol. 86, 6537–6545.

Kleinfelter, L.M., Jangra, R.K., Jae, L.T., Herbert, A.S., Mittler, E., Stiles, K.M., Wirchnianski, A.S., Kielian, M., Brummelkamp, T.R., Dye, J.M., and Chandran, K. (2015). Haploid genetic screen reveals a profound and direct dependence on cholesterol for hantavirus membrane fusion. MBio 6, e00801.

Lei, C., Qian, K., Li, T., Zhang, S., Fu, W., Ding, M., and Hu, S. (2020). Neutralization of SARS-CoV-2 spike pseudotyped virus by recombinant ACE2-Ig. Nat. Commun. 11, 2070.

Letko, M., Marzi, A., and Munster, V. (2020). Functional assessment of cell entry and receptor usage for SARS-CoV-2 and other lineage B betacoronaviruses. Nat. Microbiol. 5, 562–569.

Limburg, H., Harbig, A., Bestle, D., Stein, D.A., Moulton, H.M., Jaeger, J., Janga, H., Hardes, K., Koepke, J., Schulte, L., et al. (2019). TMPRSS2 is the major activating protease of influenza A virus in primary human airway cells and influenza B virus in human type II pneumocytes. J. Virol. 93, e00649-19.

Liu, R., Wang, J., Shao, Y., Wang, X., Zhang, H., Shuai, L., Ge, J., Wen, Z., and Bu, Z. (2018). A recombinant VSV-vectored MERS-CoV vaccine induces neutralizing antibody and T cell responses in rhesus monkeys after single dose immunization. Antiviral Res. 150, 30–38.

Maier, K.E., Jangra, R.K., Shieh, K.R., Cureton, D.K., Xiao, H., Snapp, E.L., Whelan, S.P., Chandran, K., and Levy, M. (2016). A new transferrin receptor aptamer inhibits new world hemorrhagic fever mammarenavirus entry. Mol. Ther. Nucleic Acids 5, e321.

McBride, C.E., Li, J., and Machamer, C.E. (2007). The Cytoplasmic Tail of the Severe Acute Respiratory Syndrome Coronavirus Spike Protein Contains a Novel Endoplasmic Reticulum Retrieval Signal That Binds COPI and Promotes Interaction with Membrane Protein. Journal of Virology 81, 2418–2428.

Morgenstern, J.P., and Land, H. (1990). Advanced mammalian gene transfer: high titre retroviral vectors with multiple drug selection markers and a complementary helper-free packaging cell line. Nucleic Acids Res. 18, 3587–3596.

Mossel, E.C., Huang, C., Narayanan, K., Makino, S., Tesh, R.B., and Peters, C.J. (2005). Exogenous ACE2 expression allows refractory cell lines to support severe acute respiratory syndrome coronavirus replication. J. Virol. 79, 3846–3850.

Nie, J., Li, Q., Wu, J., Zhao, C., Hao, H., Liu, H., Zhang, L., Nie, L., Qin, H., Wang, M., et al. (2020). Establishment and validation of a pseudovirus neutralization assay for SARS-CoV-2. Emerg. Microbes Infect. 9, 680–686.

Nimishakavi, S., Raymond, W.W., Gruenert, D.C., and Caughey, G.H. (2015). Divergent Inhibitor Susceptibility among Airway Lumen-Accessible Tryptic Proteases. PLoS One 10, e0141169.

NYU Langone Health/Albert Einstein College of Medicine (2020). Convalescent Plasma to Limit COVID-19 Complications in Hospitalized Patients. ClinicalTrials.gov Identifier: NCT04364737, Retrieved on May, 19th 2020 https://clinicaltrials.gov/ct2/show/NCT04364737?term=Montefiore&cond=COVID-19&draw=2&rank=2.

Ou, X., Liu, Y., Lei, X., Li, P., Mi, D., Ren, L., Guo, L., Guo, R., Chen, T., Hu, J., et al. (2020). Characterization of spike glycoprotein of SARS-CoV-2 on virus entry and its immune cross-reactivity with SARS-CoV. Nat. Commun. 11, 1620.

Pettersen, E.F., Goddard, T.D., Huang, C.C., Couch, G.S., Greenblatt, D.M., Meng, E.C., and Ferrin, T.E. (2004). UCSF Chimera–a visualization system for exploratory research and analysis. J. Comput. Chem. 25, 1605–1612.

Pinto, D., Park, Y.-J., Beltramello, M., Walls, A.C., Tortorici, M.A., Bianchi, S., Jaconi, S., Culap, K., Zatta, F., De Marco, A., et al. (2020). Cross-neutralization of SARS-CoV-2 by a human monoclonal SARS-CoV antibody. Nature 583, 290–295.

Pu, T., Ding, C., Li, Y., Liu, X., Li, H., Duan, J., Zhang, H., Bi, Y., and Cun, W. (2020). Evaluate severe acute respiratory syndrome coronavirus 2 infectivity by pseudoviral particles. J. Med. Virol. https://doi.org/10.1002/jmv.25865.

Raaben, M., Jae, L.T., Herbert, A.S., Kuehne, A.I., Stubbs, S.H., Chou, Y.-Y., Blomen, V.A., Kirchhausen, T., Dye, J.M., Brummelkamp, T.R., and Whelan, S.P. (2017). NRP2 and CD63 are host factors for lujo virus cell entry. Cell Host Microbe 22, 688–696.e5.

Rockx, B., Kuiken, T., Herfst, S., Bestebroer, T., Lamers, M.M., Oude Munnink, B.B., de Meulder, D., van Amerongen, G., van den Brand, J., Okba, N.M.A., et al. (2020). Comparative pathogenesis of COVID-19, MERS, and SARS in a nonhuman primate model. Science 368, 1012–1015.

Rogers, T.F., Zhao, F., Huang, D., Beutler, N., Burns, A., He, W.T., Limbo, O., Smith, C., Song, G., Woehl, J., et al. (2020). Isolation of potent SARS-CoV-2 neutralizing antibodies and protection from disease in a small animal model. Science, eabc7520, https://doi.org/10.1126/science.abc7520.

Shang, J., Ye, G., Shi, K., Wan, Y., Luo, C., Aihara, H., Geng, Q., Auerbach, A., and Li, F. (2020a). Structural basis of receptor recognition by SARS-CoV-2. Nature 581, 221–224.

Shang, J., Wan, Y., Luo, C., Ye, G., Geng, Q., Auerbach, A., and Li, F. (2020b). Cell entry mechanisms of SARS-CoV-2. Proc. Natl. Acad. Sci. USA 117, 11727–11734.

Shen, L.W., Mao, H.J., Wu, Y.L., Tanaka, Y., and Zhang, W. (2017). TMPRSS2: A potential target for treatment of influenza virus and coronavirus infections. Biochimie 142, 1–10.

Slough, M.M., Chandran, K., and Jangra, R.K. (2019). Two point mutations in old world hantavirus glycoproteins afford the generation of highly infectious recombinant vesicular stomatitis virus vectors. MBio 10, e02372-18.

Stadlbauer, D., Amanat, F., Chromikova, V., Jiang, K., Strohmeier, S., Arunkumar, G.A., Tan, J., Bhavsar, D., Capuano, C., Kirkpatrick, E., et al. (2020). SARS-CoV-2 Seroconversion in Humans: A Detailed Protocol for a Serological Assay, Antigen Production, and Test Setup. Curr. Protoc. Microbiol. 57, e100.

Stewart, S.A., Dykxhoorn, D.M., Palliser, D., Mizuno, H., Yu, E.Y., An, D.S., Sabatini, D.M., Chen, I.S.Y., Hahn, W.C., Sharp, P.A., et al. (2003). Lentivirus-delivered stable gene silencing by RNAi in primary cells. RNA 9, 493–501.

Tan, C.W., Chia, W.N., Chen, M.I.-C., Hu, Z., Young, B.E., Tan, Y.-J., Yi, Y., Lye, D.C., Anderson, D.E., and Wang, L.-F. (2020). A SARS-CoV-2 surrogate virus neutralization test (sVNT) based on antibody-mediated blockage of ACE2-spike (RBD) protein-protein interaction. 10.1002/jmv.25865.

Ujike, M., Huang, C., Shirato, K., Makino, S., and Taguchi, F. (2016). The contribution of the cytoplasmic retrieval signal of severe acute respiratory syndrome coronavirus to intracellular accumulation of S proteins and incorporation of S protein into virus-like particles. Journal General Virology 97, 1853–1864.

Walls, A.C., Park, Y.-J., Tortorici, M.A., Wall, A., McGuire, A.T., and Veesler, D. (2020). Structure, Function, and Antigenicity of the SARS-CoV-2 Spike Glycoprotein. Cell *181*, 281–292.e6.

Wang, Q., Zhang, Y., Wu, L., Niu, S., Song, C., Zhang, Z., Lu, G., Qiao, C., Hu, Y., Yuen, K.-Y., et al. (2020). Structural and Functional Basis of SARS-CoV-2 Entry by Using Human ACE2. Cell *181*, 894–904.e9.

Wec, A.Z., Wrapp, D., Herbert, A.S., Maurer, D.P., Haslwanter, D., Sakharkar, M., Jangra, R.K., Dieterle, M.E., Lilov, A., Huang, D., et al. (2020). Broad neutralization of SARS-related viruses by human monoclonal antibodies. Science, eabc7424, https://doi.org/10.1126/science.abc7424.

Whelan, S.P., Ball, L.A., Barr, J.N., and Wertz, G.T. (1995). Efficient recovery of infectious vesicular stomatitis virus entirely from cDNA clones. Proc. Natl. Acad. Sci. USA *92*, 8388–8392.

Witko, S.E., Kotash, C.S., Nowak, R.M., Johnson, J.E., Boutilier, L.A.C., Melville, K.J., Heron, S.G., Clarke, D.K., Abramovitz, A.S., Hendry, R.M., et al. (2006). An efficient helper-virus-free method for rescue of recombinant paramyxoviruses and rhadoviruses from a cell line suitable for vaccine development. J. Virol. Methods *135*, 91–101.

Wong, A.C., Sandesara, R.G., Mulherkar, N., Whelan, S.P., and Chandran, K. (2010). A forward genetic strategy reveals destabilizing mutations in the Ebolavirus glycoprotein that alter its protease dependence during cell entry. J. Virol. *84*, 163–175.

World Health Organization (2020). Situation report-147, Coronavirus disease (COVID-19), Retrieved on June 15th, 2020 https://www.who.int/docs/default-source/coronaviruse/situation-reports/20200615-covid-19-sitrep-147.pdf?sfvrsn=2497a605_2.

Wrapp, D., Wang, N., Corbett, K.S., Goldsmith, J.A., Hsieh, C.-L., Abiona, O., Graham, B.S., and McLellan, J.S. (2020). Cryo-EM structure of the 2019-nCoV spike in the prefusion conformation. Science *367*, 1260–1263.

Wu, F., Zhao, S., Yu, B., Chen, Y.-M., Wang, W., Song, Z.-G., Hu, Y., Tao, Z.-W., Tian, J.-H., Pei, Y.-Y., et al. (2020a). A new coronavirus associated with human respiratory disease in China. Nature *579*, 265–269.

Wu, Y., Wang, F., Shen, C., Peng, W., Li, D., Zhao, C., Li, Z., Li, S., Bi, Y., Yang, Y., et al. (2020b). A noncompeting pair of human neutralizing antibodies block COVID-19 virus binding to its receptor ACE2. Science *368*, 1274–1278.

Xiong, H.-L., Wu, Y.-T., Cao, J.-L., Yang, R., Ma, J., Qiao, X.-Y., Yao, X.-Y., Zhang, B.-H., Zhang, Y.-L., Hou, W.-H., et al. (2020). Robust neutralization assay based on SARS-CoV-2 S-bearing vesicular stomatitis virus (VSV) pseudovirus and ACE2-overexpressed BHK21 cells. bioRxiv. https://doi.org/10.1101/2020.04.08.026948.

Yang, X., Dong, N., Chan, W.-C., and Chen, S. (2020). Identification of super-transmitters of SARS-CoV-2 (MedRxiv). https://doi.org/10.1101/2020.04.19.20071399.

Zang, R., Gomez Castro, M.F., McCune, B.T., Zeng, Q., Rothlauf, P.W., Sonnek, N.M., Liu, Z., Brulois, K.F., Wang, X., Greenberg, H.B., et al. (2020). TMPRSS2 and TMPRSS4 promote SARS-CoV-2 infection of human small intestinal enterocytes. Sci. Immunol. *5*, eabc3582.

Zhou, Y., Vedantham, P., Lu, K., Agudelo, J., Carrion, R., Jr., Nunneley, J.W., Barnard, D., Pöhlmann, S., McKerrow, J.H., Renslo, A.R., and Simmons, G. (2015). Protease inhibitors targeting coronavirus and filovirus entry. Antiviral Res. *116*, 76–84.

Zhou, P., Yang, X.L., Wang, X.G., Hu, B., Zhang, L., Zhang, W., Si, H.R., Zhu, Y., Li, B., Huang, C.L., et al. (2020). A pneumonia outbreak associated with a new coronavirus of probable bat origin. Nature *579*, 270–273.

Zost, S.J., Gilchuk, P., Chen, R.E., Case, J.B., Reidy, J.X., Trivette, A., Nargi, R.S., Sutton, R.E., Suryadevara, N., Chen, E.C., et al. (2020). Rapid isolation and profiling of a diverse panel of human monoclonal antibodies targeting the SARS-CoV-2 spike protein. bioRxiv. 2020.05.12.091462. https://doi.org/10.1101/2020.05.12.091462.

STAR★METHODS

KEY RESOURCES TABLE

REAGENT or RESOURCE	SOURCE	IDENTIFIER
Antibodies		
Goat hACE2-specific antibody	R&D systems	Cat# AF933 RRID: AB_355722
Rabbit Coronavirus Nucleocapsid Antibody	SinoBiological	Cat# 40143-R001 RRID: AB_2827974
Goat AlexaFluor 488-conjugated anti-Rabbit IgG	ThermoFisher	Cat# A32731 RRID: AB_2633280
Human gamma globulin	Jackson ImmunoResearch	Cat# 009-000-002 RRID: AB_2337042
Donkey AlexaFluor 594-conjugated anti-goat IgG	Invitrogen	Cat# A32758 RRID: AB_2762828
Goat anti-human IgG-HRP	Invitrogen	Cat# 31410 RRID: AB_228269
Bacterial and Virus Strains		
SARS-CoV-2 (Washington State isolate)	USAMRIID	MT020880.1
rVSV-EBOV/Mayinga GP (EBOV/H.sap-tc/COD/76/Yambuku-Mayinga)	(Wong et al., 2010)	N/A
rVSV- G	(Whelan et al., 1995)	N/A
rVSV-SARS-CoV-2 S (Wuhan-Hu-1 isolate)	This study	A passage 9 viral stock will be distributed for *in vitro* non-commercial use under a UBMTA.
Biological Samples		
Antisera from COVID-19 convalescent donors obtained with IRB approval and informed consent	This study	N/A
Chemicals, Peptides, and Recombinant Proteins		
Cysteine cathepsin inhibitor E-64	Wako Chemicals	Cat# 331-40963
Camostat mesylate	Tocris	Cat# 3193
Cathepsin L/B inhibitor Z-Phe-tyr-dmk	Calbiochem	Cat# 219427
Ammonium chloride	Acros organics	Cat# 123340010
Ultra-TMB colorimetric substrate	Thermo Fisher	Cat# 34029
Critical Commercial Assays		
RNeasy Mini Kit (250)	QIAGEN	Cat# 7410
SuperScript™ IV Reverse Transcriptase	Invitrogen	Cat# 18090050
Deposited Data		
Does not apply	-	-
Experimental Models: Cell Lines		
Human hepatoma Huh7.5.1	Laboratory of Dr. Jan Carrette (Originally from Dr. Frank Chisari)	N/A
293FT	ThermoFisher	*Cat# R70007RRID: CVCL_6911*
Vero	ATCC	CCL-81 RRID: CVCL_0059
Vero-TMPRSS2	This study	N/A
Vero C1008 cells (VERO 76, clone E6, Vero E6)	ATCC	CRL-1586 RRID: CVCL_0574
ExpiCHO-S cells	ThermoFisher	Cat# A29127
BHK21 [C13]	Laboratory of Dr. Margaret Kielian /ATCC	CCL10 RRID: CVCL_1915

Continued

REAGENT or RESOURCE	SOURCE	IDENTIFIER
BHK21-hACE2	This study	N/A
FreeStyle 293F	ThermoFisher	Cat# R79007
Calu3	Laboratory of Dr. Simon Anthony/ ATCC	HTB-55 RRID: CVCL_0609
A549	Laboratory of Dr. Balaji Manicassamny/ ATCC	CCL-185 RRID: CVCL_0023
Experimental Models: Organisms/Strains		
Does not apply	-	-
Oligonucleotides		
MluI-nSARS-CoV-2 S-F CAGAGATCGATCTGTTTCCTTGACACGC GTGCCACCATGTTCGTGTTCCTG	IDT	N/A
NotI-nSARS-CoV-2 S-R GTTCAAACATGAAG AATCTGTGTGCAGGGCGGCCGCTCAGGT GTAGTGCAGCTTCACG	IDT	N/A
S-549F (rVSV SARS-CoV-2 S -Sanger sequencing) GGCAACTTCAAGAACCTGA GA	IDT	N/A
S-1159F (rVSV SARS-CoV-2 S -Sanger sequencing) TGAATGACCTGTGCTTCACC	IDT	N/A
S-1758F (rVSV SARS-CoV-2 S -Sanger sequencing) ATTACACCCTGCTCCTTCGG	IDT	N/A
S-2357F (rVSV SARS-CoV-2 S -Sanger sequencing) GCAGATCTACAAGACCCCACC	IDT	N/A
S-2946F (rVSV SARS-CoV-2 S -Sanger sequencing) AGACTGGACAAGGTGGAAGC	IDT	N/A
VSV-2860F (rVSV SARS-CoV-2 S -Sanger sequencing) AGGCCTTAATGTTTGGCCTG	IDT	N/A
VSV-4773R (rVSV SARS-CoV-2 S -Sanger sequencing) AAATCATTGAACTCGTCGGTCTC	IDT	N/A
Recombinant DNA		
Plasmid: VSV antigenome plasmid	(Whelan et al., 1995)	N/A
Plasmids: plasmids expressing T7 polymerase and VSV N, P, M, G and L	(Witko et al., 2006)	N/A
Plasmid: pBabe-puro-hACE2	This study	N/A
Plasmid: pBabe-puro-TMPRSS2	This study	N/A
Plasmid: pBabe-puro	(Morgenstern and Land, 1990)	Addgene plasmid # 1764
Plasmid: VSV-G	(Stewart et al., 2003)	Addgene plasmid # 8454
Plasmid: pUMVC	(Stewart et al., 2003)	Addgene plasmid # 8449
Plasmid: pCAGGS SARS-CoV-2 Spike	Laboratory of Dr. Jason McLellan	N/A
Plasmid: pCAGGS SARS-CoV-2 RBD	Laboratory of Dr. Florian Krammer (BEI resources)	Cat# NR-52366
Synthetic, codon-optimized (humanized) SARS-2-CoV-2 S GenBank MN908947.3	TwistBioscience	N/A
Plasmid: hACE2	Laboratory of Dr. Hyeryun Choe	Addgene plasmid #1786
Plasmid: TMPRSS2	Laboratory of Dr. Roger Reeves	Addgene plasmid #53887
Software and Algorithms		
GraphPad Prism (version 8.3.0(538))	GraphPad Software	https://www.graphpad.com/
Adobe Photoshop (version 21.1.3)	Adobe	https://www.adobe.com/
Adobe Illustrator (version 24.1.3)	Adobe	https://www.adobe.com/
Pymol 2.4	Schrödinger, LLC	https://pymol.org/2/

Continued

REAGENT or RESOURCE	SOURCE	IDENTIFIER
UCSF Chimera	(Pettersen et al., 2004)	https://www.cgl.ucsf.edu/chimera/
SnapGene	SnapGene	https://www.snapgene.com/
Other		
Zeiss Axio Observer.Z1 inverted fluorescence microscope	Carl Zeiss AG	N/A
Cytation 5 Cell Imaging Multi-Mode Reader	BioTek	N/A
Operetta High Content Imaging System	Perkin Elmer	N/A

RESOURCE AVAILABILITY

Lead Contact
Further information and requests for resources and reagents should be directed to and will be fulfilled by the Lead Contact, Kartik Chandran (kartik.chandran@einsteinmed.org).

Materials Availability
Plasmids and a passage 9 stock of rVSV-SARS-CoV-2 S generated in this study, together with documenting information, will be made available upon request and following execution of a UBMTA between Albert Einstein College of Medicine and the recipient institution. rVSV-SARS-CoV-2 S will be made available for *in vitro* research only (please see the 'Limitations of the Study' section).

Data and Code Availability
Primary data are available on request. This study did not generate any new software code.

EXPERIMENTAL MODEL AND SUBJECT DETAILS

Cells
Human hepatoma Huh7.5.1 (received from Dr. Jan Carette; originally from Dr. Frank Chisari) and 293FT (ThermoFisher) cells were cultured in Dulbecco's Modified Eagle Medium (DMEM high glucose, GIBCO) supplemented with 10% heat-inactivated fetal bovine serum (FBS, Atlanta Biologicals), 1% Penicillin/Streptomycin (P/S, GIBCO) and 1% Gluta-MAX (GIBCO). The African vervet monkey kidney Vero cells and baby hamster kidney BHK21 cells were maintained in DMEM (high glucose) supplemented with 2% heat-inactivated FBS, 1% P/S and 1% Gluta-MAX. Vero-E6 cells were grown in Minimum Essential Medium (MEM) supplemented in 10% FBS and Gentamicin (all from Sigma). A549 cells were maintained in DMEM (high glucose) supplemented with 10% heat-inactivated FBS, 1% P/S and 1% Gluta-MAX. These cell lines were passaged every 2-3 days using 0.05% Trypsin/EDTA solution (GIBCO). Calu3 cells were cultured in Eagle's Minimum Essential Medium (EMEM, ATCC) supplemented with 10% heat-inactivated FBS, 1% P/S, and 1% Gluta-MAX and passaged weekly using 0.05% Trypsin/EDTA solution.

Generation of Cells Overexpressing hACE2 or TMPRSS2
Human ACE2 and TMPRSS2 coding sequences were PCR-amplified from the hACE2 plasmid Addgene #1786 (a generous gift from Hyeryun Choe) and TMPRSS2 plasmid Addgene #53887 (a generous gift from Roger Reeves), respectively and cloned into a retro-viral pBabe-puro vector. Retroviruses were produced by transfecting 293FT cells with the hACE2 and TMPRSS2 expressing pBabe-puro plasmids along with those expressing the Moloney murine leukemia virus (MMLV) gag-pol and VSV G proteins. Retroviral supernatants passed through a 0.45-μm filter were used to transduce BHK21, Vero cells or A549 cells. Transfected cells were selected with puromycin (2 μg/mL).

Convalescent Serum Samples
Serum samples were collected from healthy adult volunteers residing in Westchester County, NY who had recovered from COVID-19 in April 2020. Patients had reported a positive nasopharyngeal swab by PCR for SARS-CoV-2 during illness and had been asymptomatic for at least 14 days prior to sample collection. After obtaining informed consent, serum was obtained by venipuncture (BD Vacutainer, serum), centrifuged, aliquoted and stored at $-80°C$ prior to use. The sera were heat-inactivated at $56°C$ for 30 min and stored at $4°C$ prior to analysis. Protocol approval was obtained by the Institutional Review Board (IRB) of the Albert Einstein College of Medicine.

Generation of rVSV-SARS-CoV-2
A plasmid encoding the VSV antigenome was modified to replace its native glycoprotein, G, with the full-length wild-type *S* glycoprotein gene of the Wuhan-Hu-1 isolate of SARS-CoV-2 (GenBank MN908947.3). The VSV antigenome also encodes for an eGFP reporter gene as a separate transcriptional unit. Plasmid-based rescue of the rVSV was carried out as described previously (Klein-

felter et al., 2015; Whelan et al., 1995; Wong et al., 2010). Briefly, 293FT cells were transfected with the VSV antigenome plasmid along with plasmids expressing T7 polymerase and VSV N, P, M, G and L proteins by using polyethylenimine. Supernatants from the transfected cells were transferred to Huh7.5.1 cells every day (day 2-7 post-transfection) till the appearance of eGFP-positive cells. The poorly spreading virus was initially propagated by cell subculture. RNA was isolated from viral supernatants at different passages and Sanger sequencing was used to verify *S* gene sequences. A passage #9 viral stock was plaque-purified on Vero cells. Supernatants were aliquoted and stored at −80°C. The generation of rVSV-SARS-CoV-2 S and its use in tissue culture at biosafety level 2 was approved by the Environmental Health and Safety Department and the Institutional Biosafety Committee at Albert Einstein College of Medicine.

SARS-CoV-2 Stock Preparation

All work with authentic SARS-CoV-2 was completed in BSL-3 laboratories at USAMRIID in accordance with federal and institutional biosafety standards and regulations. Vero-76 cells were inoculated with SARS-CoV-2 (GenBank MT020880.1) at a MOI = 0.01 and incubated at 37°C with 5% CO_2 and 80% humidity. At 50 h post-infection, cells were frozen at −80°C for 1 h, allowed to thaw at room temperature, and supernatants were collected and clarified by centrifugation at ∼2,500 × g for 10 min. Clarified supernatant was aliquoted and stored at −80°C. Sequencing data from this virus stock indicated a single mutation in the spike glycoprotein (H655Y) relative to Washington state isolate MT020880.1.

SARS-CoV2 Spike Glycoprotein RBD Expression and Purification

The pCAGGS SARS-CoV2 RBD plasmid (a generous gift from Florian Krammer) was used for the expression of recombinant RBD as previously described (Amanat et al., 2020; Stadlbauer et al., 2020). FreeStyle 293F cells (ThermoFisher Scientific) were transfected with the plasmid DNA diluted in PBS (0.67 μg total plasmid DNA per ml of culture) using polyethylenimine (Polysciences, Inc.) at a DNA-to-PEI ratio of 1:3. At 6 days post-transfection, cultures were harvested by centrifugation at 4,000 x g for 20 min, and supernatant was incubated with Ni-NTA resin (GoldBio) for 2 h at 4°C. Resin was collected in columns by gravity flow, washed with a wash buffer (50 mM Tris HCl pH 8.0, 250 mM NaCl, 20 mM Imidazole) and eluted with an elution buffer (50 mM Tris HCl pH 8.0, 250 mM NaCl, 250 mM Imidazole). Eluant was concentrated in Amicon centrifugal units (EMD Millipore) and buffer was exchanged into the storage buffer (50 mM Tris HCl pH 8.0, 250 mM NaCl). Protein was analyzed by SDS-PAGE, aliquoted, and stored at −80°C.

SARS-CoV2 Spike Glycoprotein Expression and Purification

The pCAGGS SARS-CoV2 plasmid encoding stabilized *S* glycoprotein gene (a generous gift from Jason McLellan) was used for the expression of recombinant S protein as described previously (Wrapp et al., 2020) with several modifications. ExpiCHO-S cells (ThermoFisher) were transiently transfected with plasmid DNA diluted in OptiPRO Serum-Free Medium (0.8 μg total DNA per ml of culture) using ExpiFectamine (ThermoFisher) at a DNA-to-ExpiFectamine ratio of 1:4. At 8 days post-transfection, cultures were harvested by centrifugation at 4,000 x g for 20 min. Clarified supernatant was dialyzed in 50 mM Tris HCl pH 8.0, 250 mM NaCl at a clarified supernatant to dialysis buffer ratio of 1:25 prior affinity chromatography. Dialyzed supernatant was incubated with Ni-NTA resin (GoldBio) for 2 h at 4°C. Resin was collected in columns by gravity flow, washed with wash buffer (50 mM Tris HCl pH 8.0, 250 mM NaCl, 20 mM Imidazole) and eluted with elution buffer (50 mM Tris HCl pH 8.0, 250 mM NaCl, 250 mM Imidazole). Eluate was concentrated in Amicon centrifugal units (EMD Millipore) and exchanged into a storage buffer (50 mM Tris HCl pH 8.0, 250 mM NaCl). Protein was analyzed by SDS-PAGE, aliquoted, and stored at −80°C.

METHOD DETAILS

Detection of S Protein in rVSV-SARS-CoV-2

High-protein binding 96-well ELISA plates (Corning) were coated with 25 μl of concentrated rVSV-SARS-CoV-2 S or rVSV-EBOV (2.73 μg/mL) overnight at 4°C, and blocked with 3% nonfat dry milk in PBS (PBS-milk) for 1 h at 25°C. Plates were extensively washed and incubated with serum 18, serum 39 or negative serum diluted to 1:100 first then with serial 2-fold dilutions in PBS milk 1% -Tween 0.1% for 1 h at 25°C. Plates were washed three times and incubated with Goat anti-human IgG-HRP (#31410 Invitrogen) diluted 1:3000 (PBS milk 1% -Tween 0.1%) for 1 h at 25°C and detected using 1-Step Ultra TMB-ELISA Substrate Solution (Thermo Fisher Scientific, Waltham, MA). Plates were read using a Cytation 5 imager (BioTek) at 450 nm.

NH₄Cl Inhibition Experiments

Huh7.5.1 cell monolayers were incubated for 1 h with 20–100 mM NH_4Cl in DMEM. Next, pre-titrated rVSVs expressing EBOV GP or SARS-CoV-2 S were used to infect cells. Infection was scored 16-18 h later as described above.

Cathepsin Inhibitor Experiments

Monolayers of Vero cells pre-treated for 1.5 h at 37°C with E-64 (37.5 or 75 μM), Z-Phe-tyr-dmk (FYdmk, 18.75 or 37.5 μM), or 1.5% DMSO (vehicle control) were infected with pre-titrated amounts of rVSVs carrying SARS-CoV 2 S, EBOV GP or VSV G. At 1 h post-infection, 20 mM NH_4Cl was added. Infected cells were fixed 16–18 h later and scored for infection as described above.

TMPRSS2 Inhibitor Experiments

Monolayers of Vero or Vero-TMPRSS2 cells pre-treated for 2 h at 37°C with camostat mesylate (Tocris) or 1% DMSO (vehicle control) were infected with pre-titrated amounts of rVSV-SARS-CoV 2 S. At 1 h post-infection, 20 mM NH_4Cl was added to terminate viral entry. Infected cells were fixed 7 h later and scored for infection as described above.

Detection of hACE2 in BHK21 and A549 Transfected Cells

To stain for surface-expressed hACE2, BHK21, A549, BHK21-hACE2 and A549-hACE2 cells or the control cells were seeded onto fibronectin-coated glass coverslips were incubated with 0.4 μg/mL of hACE2-specific goat antibody (#AF933, R&D systems) at 4°C in media containing 25 mM HEPES. Next, cells were washed with cold PBS, fixed with 4% paraformaldehyde, and blocked with buffer (2% (w/v) bovine serum albumin, 5% (v/v) glycerol, 0.2% (v/v) Tween20 in Ca^{2+}/Mg^{2+}-free PBS). Secondary donkey AlexaFluor 594-conjugated anti-goat IgG (#A32758 Invitrogen) was used to detect the hACE2 signal. Coverslips were mounted in Prolong with DAPI (Invitrogen) and imaged on an Axio Observer inverted microscope (Zeiss).

rVSV-SARS-CoV-2 S Microneutralization Assay

Serum samples were serially diluted and incubated with virus for 1 h at room temperature. Serum-virus mixtures were then added in duplicate to 384-well plates (Corning) containing Huh7.5.1 cells or 96-well plates (Corning) containing Vero cells. Plates were incubated for 7 h at 37°C and 5% CO2. Cells were fixed with 4% paraformaldehyde (Sigma), washed with PBS, and stored in PBS containing Hoechst-33342 (Invitrogen) at a dilution of 1:2,000. Viral infectivity was measured by automated enumeration of GFP-positive cells from captured images using a Cytation5 automated fluorescence microscope (BioTek) and analyzed using the Gen5 data analysis software (BioTek). The half-maximal inhibitory concentration (IC_{50}) of the mAbs was calculated using a nonlinear regression analysis with GraphPad Prism software.

Anti-hACE2 Antibody Blocking Assay

Huh7.5.1 cells were seeded into a 384-well plate and Calu3 cells in a 96-well plate pre-coated with 1% gelatin/PBS, respectively. Nex day, goat anti-human ACE2 antibody (#AF933, R&D Systems) was serially diluted and applied to the cells. After 1 h incubation at 37°C and 5% CO2, cells were infected with rVSV-SARS-CoV-2 S. At 16-18 h (Huh-7.5.1) or 8 h (Calu3) post-infection, cells were fixed and scored for infection as described above. Human gamma globulin (009-000-002) purchased from Jackson ImmunoResearch was used as negative control.

RBD Competition Assay

Monolayers of Huh7.5.1 cells in a 384-well plate were incubated with serial dilutions of recombinant RBD domain for 1 h at 37°C and 5% CO2. Cells were then infected with pre-titrated amounts of rVSV-SARS-CoV-2 or rVSV-EBOV GP and scored for infection 16–18 h later.

S-Mediated Antibody Depletion Assay

High-protein binding 96-well ELISA plates (Corning) coated with PBS alone or with 2 μg/mL of SARS-CoV-2 S protein in PBS overnight at 4°C were blocked for 1 h with 3% nonfat dry milk (Biorad) in PBS. Serum samples diluted in DMEM (1:50 dilution) were serially incubated 4 times for 1 h each at 37°C on S protein-coated or control wells. The depleted sera were tested for their neutralization capacity as described above.

SARS-CoV-2 Neutralization Assay

Serially diluted serum samples were mixed with pre-diluted SARS-CoV-2 in infection media (EMEM/2% FBS/Gentamicin) and incubated for 1 h at 37°C/5% CO2/80% humidity. Virus/serum inoculum was added to Vero-E6 cells, seeded in 96 well plates, at a MOI of 0.4 and incubated for 1 h at 37°C/5% CO2/80% humidity. Virus/serum inoculum was removed and cells were washed with PBS prior to addition of culture media (MEM/10% FBS/Gentamicin). Following 24 h incubation at 37°C/5% CO2/80% humidity, media was removed and cells were washed with PBS. PBS was removed and cells were submerged in 10% formalin for 24 h. Formalin was removed and cells were washed with PBS prior to permeabilization with 0.2% Triton-X for 10 min at room temperature. Cells were blocked for 2 h, then immunostained with SARS-1 nucleocapsid protein-specific antibody (Sino Biologic; Cat# 40143-R001) and AlexaFluor 488 labeled secondary antibody. Cells were imaged using an Operetta (Perkin Elmer) high content imaging instrument and infected cells were determined using Harmony Software (Perkin Elmer).

Syncytia Inhibition Assay

Vero cells were infected with pre-titrated amounts of rVSV-SARS-CoV-2 S for 2 h at 37°C and 5% CO2. Following the removal of virus inocula, cells were washed with PBS to remove any residual virus and indicated dilutions of convalescent sera were applied to the infected cells. Cells were fixed, their nuclei were counterstained, and syncytia formation was imaged by eGFP expression at 16 h post-infection.

QUANTIFICATION AND STATISTICAL ANALYSIS

The n number associated with each dataset in the figures indicates the number of biologically independent samples. The number of independent experiments and the measures of central tendency and dispersion used in each case are indicated in the figure legends. Dose-response neutralization curves were fit to a logistic equation by nonlinear regression analysis. Unless otherwise indicated in the figure legends, statistical comparisons were carried out by two-way ANOVA with a post hoc correction for family-wise error rate (Dunnett test for comparison of an untreated sample mean to treated sample means, Tukey test for all possible comparisons of sample means). Testing level (alpha) was 0.05 for all statistical tests. All analyses were carried out in GraphPad Prism 8.

Supplemental Information

# A Replication-Competent Vesicular Stomatitis

Virus for Studies of SARS-CoV-2

Spike-Mediated Cell Entry and Its Inhibition

M. Eugenia Dieterle, Denise Haslwanter, Robert H. Bortz III, Ariel S. Wirchnianski, Gorka Lasso, Olivia Vergnolle, Shawn A. Abbasi, J. Maximilian Fels, Ethan Laudermilch, Catalina Florez, Amanda Mengotto, Duncan Kimmel, Ryan J. Malonis, George Georgiev, Jose Quiroz, Jason Barnhill, Liise-anne Pirofski, Johanna P. Daily, John M. Dye, Jonathan R. Lai, Andrew S. Herbert, Kartik Chandran, and Rohit K. Jangra

Fig. S1
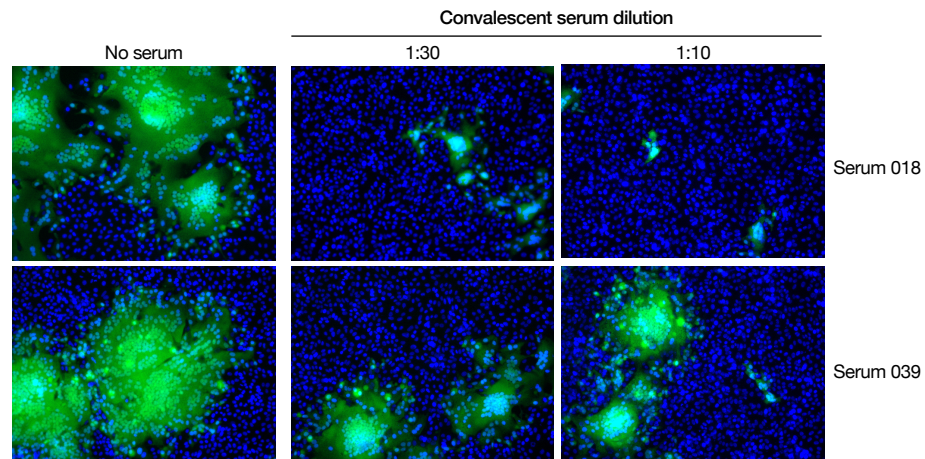
Fig S1. Inhibition of syncytium formation by sera from convalescent donors. Related to Figure 1. Vero cells were infected with pre-titrated amounts of rVSV-SARS-CoV-2. At 2 h post-infection, cells were washed with PBS to remove residual virus and then exposed to the indicated dilutions of each convalescent serum. Cells were fixed, their nuclei counterstained, and they were imaged for syncytium formation by eGFP expression at 16 h post-infection. Representative images from one of two independent experiments are shown.

SARS-CoV-2 spike trimer ectodomain
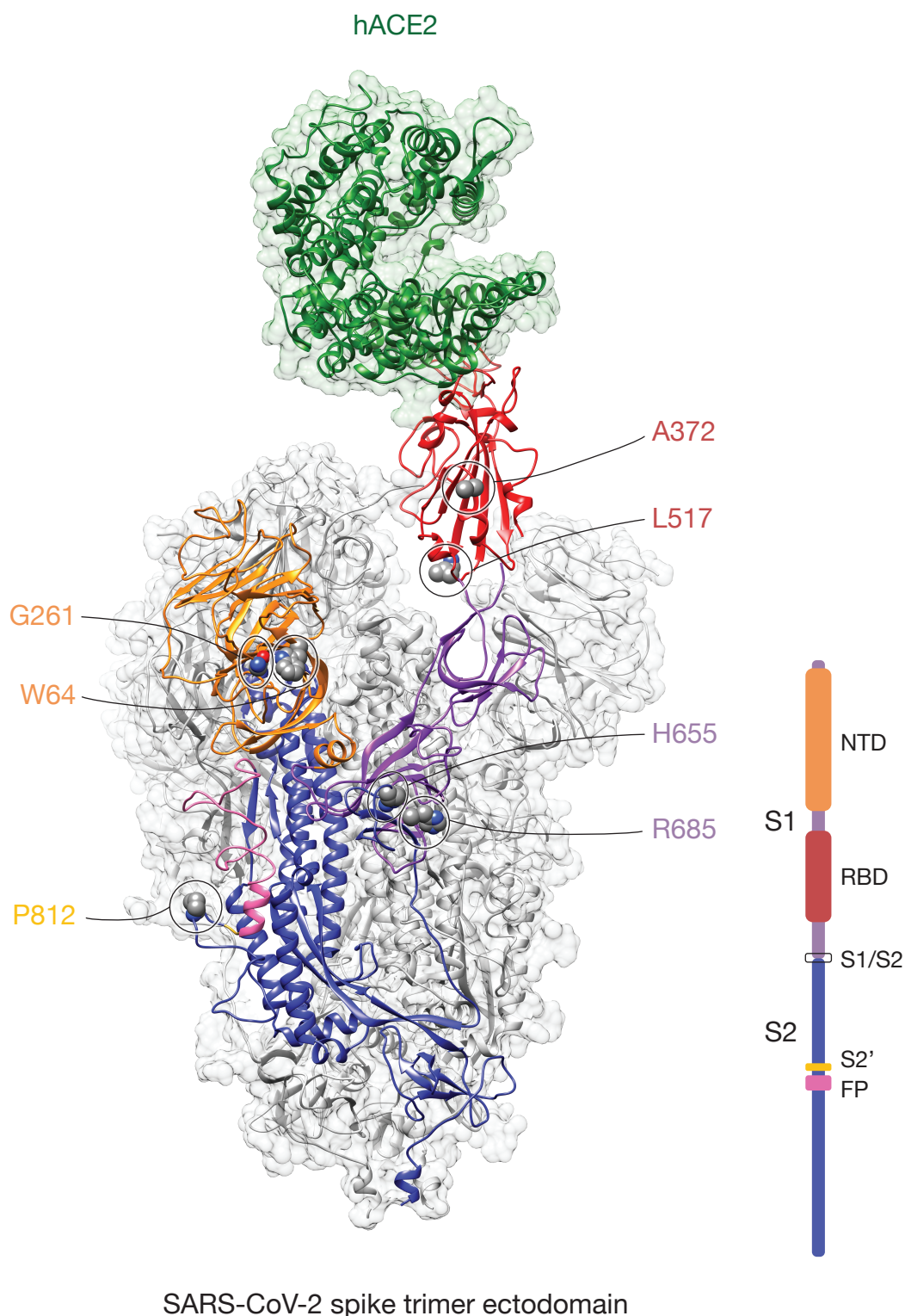
Fig S2. Locations of selected rVSV-SARS-CoV-2 S mutations in the viral spike glycoprotein. Related to Figure 1. Selected mutations (see Table S1) are indicated on a structural model of the pre-fusion confor-mation of the SARS-CoV-2 spike trimer ectodomain in complex with its receptor hACE2 (green). In order to model the SARS-CoV-2 spike trimer bound to hACE, we combined X-ray structures for the SARS-CoV-2 spike trimer (PDB IDs: 6VXX, 6VSB) with the SARS-CoV-2 S1-RBD domain bound to hACE2 (PDB IDs: 6JM0, 6LGZ) by structural superposition using Chimera. Missing loops within the spike protein were modeled using the modeller plugin in Chimera. Domains within one monomer of the spike trimer are depicted in different colors (S1: purple; S1-NTD [N–terminal domain]: orangve; S1-RBD: Red; S2: dark blue; S2-fusion peptide [FP]: yellow; S2-S2' cleavage site: pink). A linear diagram of the spike protein sequence is shown at right. NTD, N–terminal domain, RBD, receptor-binding domain. FP, fusion peptide. See text for details.
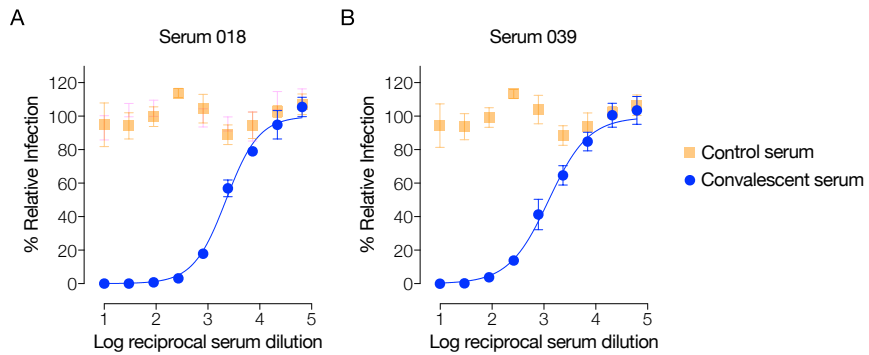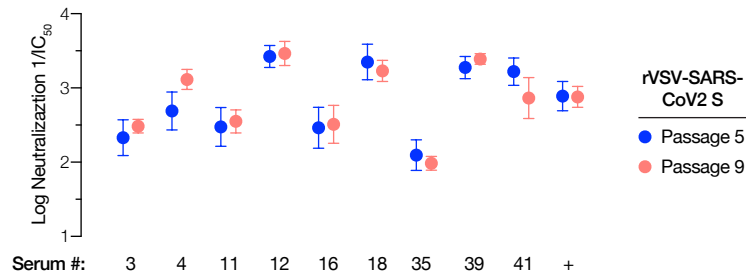
Fig S3. rVSV-SARS-CoV-2 S neutralization dose-curves with antisera from convalescent donors. Related to Figures 5 and 6. Pre-titrated amounts of rVSV-SARS-CoV-2 S were incubated with serial 3-fold dilutions of antisera from two COVID-19 convalescent donors or negative control at 37°C for 1 h. Virus:serum mixtures were then applied to monolayers of Vero cells. At 16-18 h post-infection, cells were fixed, nuclei were counterstained, and infected cells were scored for eGFP expression (Average ± SD, n = 4 from 2 independent experiments).

Fig S4. Capacities of selected convalescent antisera to neutralize two rVSV-SARS-CoV-2 S passage stocks. Related to Figure 6. Pre-titrated amounts of rVSV-SARS-CoV-2 S from passage 5 and passage 9 were incubated with serial 3-fold dilutions of antisera from nine COVID-19 convalescent donors or positive and negative controls at 37°C for 1 h. Virus:serum mixtures were then applied to monolayers of Vero cells. At 16-18 h post-infection, cells were fixed, nuclei were counterstained, and infected cells were scored for eGFP expression. IC_{50} values were extracted from logistic curve fits of the neutralization dose curves and are shown above (±95% confidence intervals).

Table S1: Spike missense and nonsense mutations acquired by rVSV-SARS-CoV-2 S during serial passage. Related to Figure 1.

.

Passage #	Mutations									
	W64R	D253N	G261R	A372T	L517S	H655Y	R685G	P812R	C1250*a	C1253*a
1										
5				X	X			X	X	X
7	X		X	X	X			X	X	X
8	X		X	X	X			X	X	X
9b	X		X	X	X			X	X	X
Plaque #1 #2	X		X	X		X	X			X
Plaque #3	X	X	X	X		X				X
Plaque #4 #5	X	X	X	X		X	X			X
Plaque #6	X		X	X			X			X

aMutation introduces stop codon.
bPlaque isolates are derived from passage 9.